universität wien

MASTERARBEIT / MASTER'S THESIS

Titel der Masterarbeit / Title of the Master's Thesis

„Transport of selected salivary biomarkers across the blood-saliva barrier in vitro "

verfasst von / submitted by

Merima Smajlhodžić-Deljo

angestrebter akademischer Grad / in partial fulfilment of the requirements for the degree of

Master of Science (MSc)

Wien, 2021/ Vienna, 2021

Studienkennzahl lt. Studienblatt / degree programme code as it appears on the student record sheet:	UA 066 834
Studienrichtung lt. Studienblatt / degree programme as it appears on the student record sheet:	Masterstudium Molekulare Biologie
Betreut von / Supervisor:	Priv.-Doz. Dipl.-Ing. Dr. Winfried Neuhaus

Declaration of academic honesty (German)

“Ich erkläre an Eides statt, dass ich die vorliegende Masterarbeit selbstständig verfasst, und in der Bearbeitung und Abfassung keine anderen als die angegebenen Quellen oder Hilfsmittel benutzt, sowie wörtliche und sinngemäße Zitate als solche gekennzeichnet habe. Die vorliegende Masterarbeit wurde noch nicht anderweitig für Prüfungszwecke vorgelegt. Ich habe mich bemüht, sämtliche Inhaber/-innen der Bildrechte ausfindig zu machen und Ihre Zustimmung zur Verwendung der Bilder in dieser Arbeit eingeholt. Sollte dennoch eine Urheberrechtverletzung bekannt werden, ersuche ich um Meldung bei mir. „

Datum: 20.08.2021.

Merima Smajlhodžić-Deljo

Acknowledgment (German)

Ich möchte mich an dieser Stelle bei allen Menschen bedanken, die während des Studiums und vor allem bei der Erstellung der Masterarbeit mich unterstützt haben. Besonderer Dank kommt meiner Mutter zu, die mir immer wieder Zuversicht gegeben hat, auch in schwierigen Phasen nicht aufzugeben und mein Ziel konsequent weiterzuverfolgen.

Einen wichtigen Beitrag leistete mein Betreuer Priv.-Doz Dipl.-Ing. Dr. Winfried Neuhaus, welcher mir durch die Stelle in seiner Arbeitsgruppe das Erstellen dieser Arbeit ermöglicht hat. Herzlichen Dank möchte ich Ihm für das Verständnis aussprechen, das er immer hatte und mich immer wieder mit der richtigen Hilfestellung auf dem richtigen Weg führte.

Ein besonderer Dank gilt Grace Lin, die mir durch technische, fachliche Unterstützung immer zur Seite stand. Dank geht auch restlichen Mitglieder der Arbeitsgruppe wie Friedl H. Peter, Anna Maria Bandian, Anna Gerhartl, Rebeka Halus, Andreas Brachner die während und abseits der Arbeit immer mir zur Seite gestanden waren.

Dankend erwähnt sei auch das Austrian Institute of Technology, in welchem die Forschungsarbeit für diese Masterarbeit unter bester technischer Unterstützung durchgeführt wurde.

Abstract (German)

Die Blut-Speichel-Schranke (BSS) als die Summe der Epithelzellschichten der Mundschleimhaut und der Speicheldrüsen definiert. Es wurde eine Vielzahl von *in vitro* Modellen der BSS entwickelt, jedoch keine endgültigen, standardisierten, zelllinienbasierten Modelle des Epithels der submandibulären Speicheldrüse. *In vitro* Modelle der BSS können eingesetzt werden, um den Transport von Biomarkern vom Blut zum Speichel zu untersuchen und zu verstehen. Das Verständnis der Funktion der Epithelbarrieren ist für eine Vielzahl von Forschungsfeldern wie Entzündungs- und Infektionskrankheiten, Gewebeverletzungen, Pharmakologie, Arzneimittelabgabe, Tumorbiologie, Zahn- und Biomarkerforschung von entscheidender Bedeutung.

Um den Transport von Biomarkern vom Blut zum Speichel zu untersuchen, haben wir daher ein epitheliales Barriere-Modell der submandibulären Speicheldrüse erstellt, das von der menschlichen Zelllinie HTB-41 (A-253), Klon B2, stammt. Transportstudien mit dem Klon B2 bestätigten seine Anwendbarkeit als Speicheldrüsenmodell für Biomarker-Studien. Zusätzlich haben wir auch ein zuvor etabliertes *in vitro* Modell der Mundschleimhaut basierend auf der Zelllinie TR146 verwendet. Entzündungen, Gewebeverletzungen, Stress und andere Krankheiten sind mit schnell erhöhten Serumspiegeln von C-reaktivem Protein (CRP) verbunden. CRP ist ein häufig verwendeter Biomarker für systemische Entzündungen, der überwiegend von der Leber synthetisiert und in Serumblutproben gemessen wird. Serum Ferritin ist als Marker für Eisenmangelanämie bekannt und wird verwendet, um den Zustand und die Schwere verschiedener Krankheiten anzuzeigen. Um das Vorhandensein eines aktiven Transports für einen dieser Biomarker (Ferritin oder CRP) über die BSS und einen Zusammenhang zwischen Blut und Speichel Konzentrationen zu untersuchen, wurden Transportstudien unter Verwendung von *in vitro* Modellen der Mundschleimhaut und der submandibulären Speicheldrüse durchgeführt. Als Ergebnis zeigten die Transportstudien mit Ferritin die Anwendbarkeit des HTB- 41 Klons B2 für diese Experimente. Für CRP wurde in beiden Modellen ein schnellerer Transport in Richtung Speichel festgestellt, was die klinische Relevanz für CRP im Speichel als nicht-invasiver Biomarker unterstreichte. Die Zugabe des löslichen Rezeptors für fortgeschrittene Glykationsendprodukte (RAGE) während des Transportes von CRP durch die BSS *in vitro* Modelle legte die Beteiligung von RAGE am CRP-Transportprozess durch die BSS vom Blut zum Speichel nahe.

Abstract (English)

The blood-saliva barrier (BSB) is defined by the sum of the epithelia of the oral mucosa and salivary glands. A variety of *in vitro* models of the BSB has been developed, but no ultimate, standardized, cell line-based models of the epithelium of the submandibular salivary gland exist. *In vitro* models of the BSB are necessary to investigate the transport of biomarkers from blood to saliva. Understanding the function of the epithelial barriers is essential for a plethora of research fields, such as, inflammation and infection diseases, tissue injury, pharmacology, drug delivery, tumor biology, dental and biomarker research.

Therefore, to study the transport of biomarkers form blood to saliva, we established an epithelial barrier model of the submandibular gland derived from human cell line HTB-41 (A-253), clone B2. Transport studies across clone B2 layers, confirmed its applicability as a salivary gland model for biomarker studies. For this work, we also used a previously established *in vitro* model of the oral mucosa based on TR146 cells.

Inflammation, tissue injury, stress and other diseases are associated with rapid increased serum levels of C-reactive protein (CRP). CRP is a commonly used biomarker of systemic inflammation, which is predominantly synthesized by the liver and measured in serum blood samples. Serum ferritin is known as a marker for iron deficiency anemia and is used to indicate the state and severity of various diseases.

To investigate the presence of an active transport for one of these biomarkers (ferritin or CRP) across the blood-saliva barrier (BSB) transport studies were performed using *in vitro* models of oral mucosa and the established model of the submandibular salivary gland. As a result, the transport studies with ferritin, demonstrated the applicability of the submandibular salivary gland model clone B2. Increased transport of CRP across both models was found in the direction from blood to saliva supporting the clinical relevance for salivary CRP as biomarker. Addition of soluble receptor for advanced glycation endproducts (RAGE) during the transport of CRP across the BSB *in vitro* models, suggested the involvement of RAGE in the CRP transport process across the BSB from blood to saliva.

Table of contents

List of figures:

List of tables:

1. INTRODUCTION

1.1. Anatomy of the oral cavity

The oral cavity, also called the mouth or the buccal cavity, is the foremost part of the digestive system of the human body and is the area of the mouth delineated by the lips, cheeks, hard palate, soft palate, and floor of mouth (Figure 1). The oral cavity consists of two regions: (I) outer oral vestibule bounded by cheeks, lips, teeth, and gingiva (gums); (II) oral cavity proper, which extends from teeth and gums back to the faces (which led to the pharynx, a part of the throat behind the mouth and nasal cavity) with the roof comprising the hard and soft palate (Ahsan, 2018).

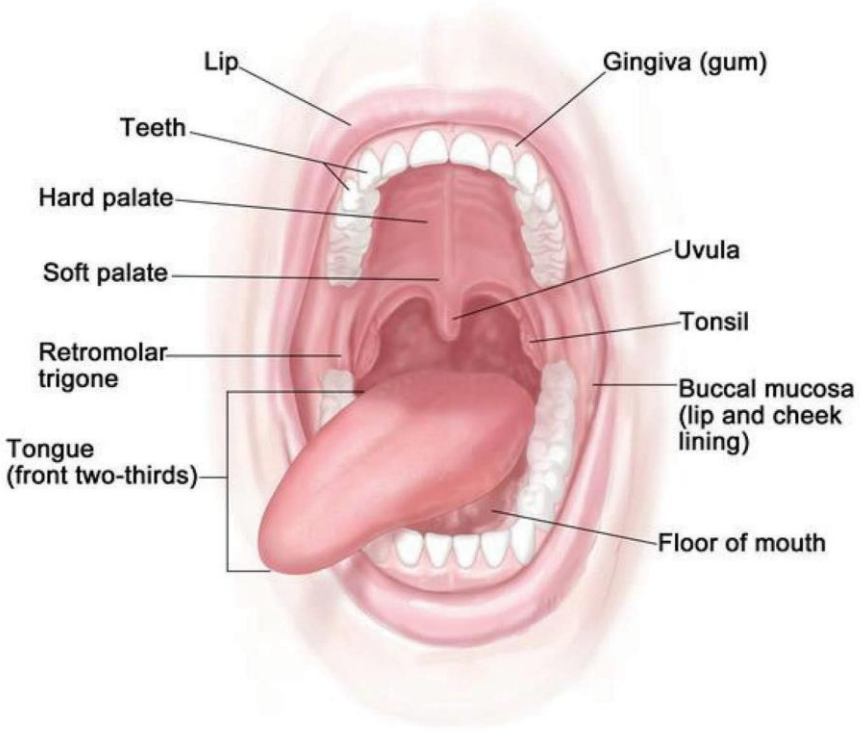

Figure 1. Anatomy of the oral cavity (For the National Cancer Institute © 2012 Terese Winslow LLC, https://visualsonline.cancer.gov/details.cfm?imageid=9259)

1.1.1. Oral mucosa

The oral mucosa protects against invading pathogens and contains an elaborate immune system. This system is thought to be pro-tolerogenic in nature as the oral mucosa remains relatively healthy (immunological homeostasis) despite the heavy microbial load (Ahsan, 2018).

The oral mucosa refers the tissue that lines the oral cavity and is composed of the masticatory, lining mucosa, and specialized mucosa (Figure 2). The masticatory mucosa forms the attached gingiva and hard palate. The lining mucosa represents the largest part of the oral mucosa, consisting of the buccal mucosa (lip and cheek lining), sublingual (floor of the mouth) and vestibular (gingiva) mucosa (Hovav, 2014).

Specialized mucosa is found on the dorsum of the tongue, involved in taste, represents 15% of the oral mucosal surface, where the masticatory mucosa represents approximately 25%, and the lining mucosa approximately 60% (Squier and Kremer, 2001).

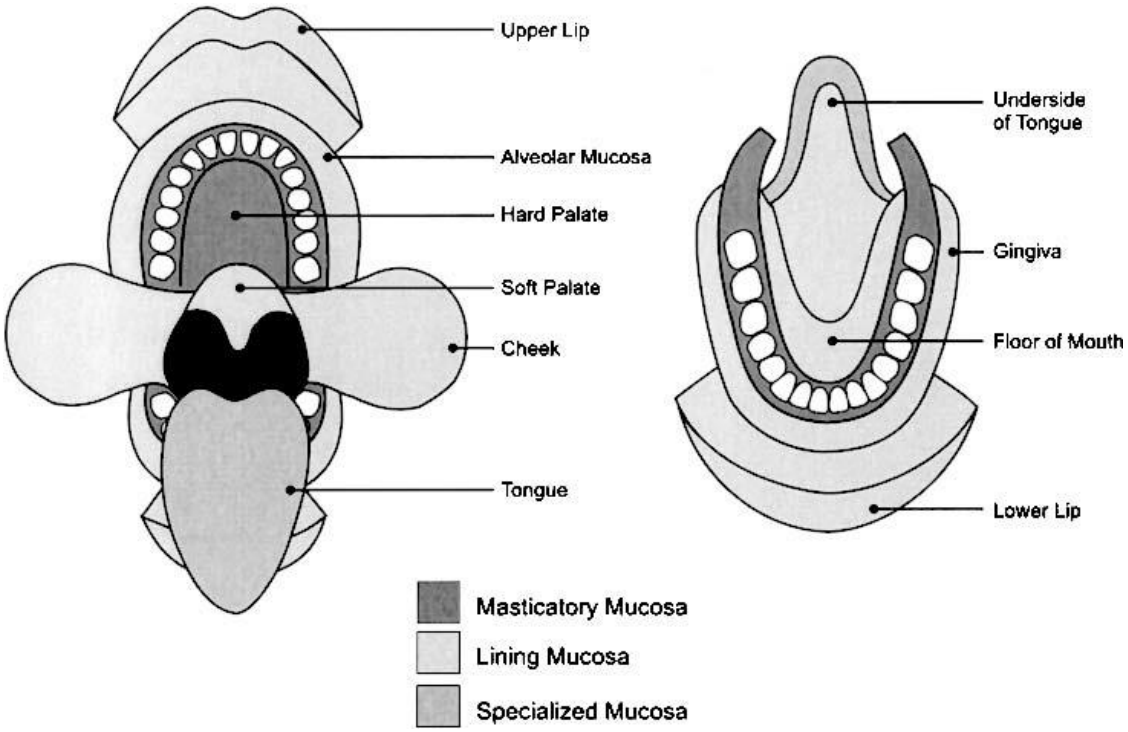

Figure 2. Schematic representation of the anatomic location of the masticatory, lining, and specialized mucosa (Patel *et al*.,2011)

The oral mucosal epithelium consists of two layers of tissues: Epithelial tissue and connective tissue (Lamina propria) followed by the submucosa as the innermost layer containing blood vessels, minor salivary glands and nerves. Between the oral epithelia and lamina propria, there is the basal membrane, which facilitates nutrition (Figure 3) (Patel *et al*.,2011).

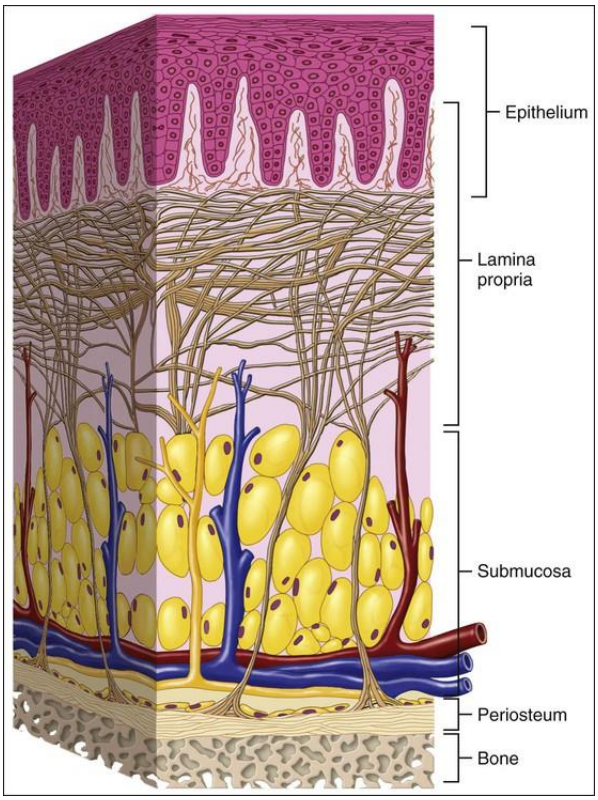

Figure 3. Structure of the human oral mucosa (Bhusnure *et al*., 2017)

The oral mucosal epithelium is a barrier that separates the underlying tissues from the environment, prevents the passage of deleterious molecules, viruses and has the ability to respond to various exogenous, possibly toxic, influences (Groeger and Meyle, 2019).

1.1.2. Salivary glands

Human salivary glands are essential organs that produce and secrete saliva, a multi-functional fluid, to the oral cavity. They are present in and around the oral cavity and their secretions play an important role in the physiological processes in the oral cavity (Punj, 2018). The salivary glands consist of three pairs of major salivary glands known as the parotid (PG), submandibular (SMG) and sublingual glands (SLG) and approximately 600-1000 minor salivary glands, distributed throughout the oral cavity (Figure 4).

The major salivary glands together are responsible for 90% of the total saliva production, and minor salivary glands secrete <10% of the total saliva, which serves as the main lubricant due to its protective and mucous components (de Paula *et al*., 2017). The anatomy of all three glands is very similar: an arborized ductal structure that opens into the oral cavity with secretory end pieces and the acini, which produce saliva (Holmberg and Hoffman, 2014). In addition to acinar cells, salivary glands consist of a complex ductal system formed by different types of ducts (intercalated, striated, and excretory ducts) and myoepithelial cells (Humphrey and Williamson, 2001).

The acinar cells are surrounded by an extracellular matrix, myoepithelial cells, stromal cells, and nerve fibers (Holmberg and Hoffman, 2014). The ducts (intercalated and striated) transport and modify the saliva from the acini, and the excretory ducts collect all fluid from the glandular lobules and secrete it to the oral cavity (de Paula *et al*., 2017). Myoepithelial cells, around acinar cells, contract after stimulation which contribute to salivary secretion into the ducts (Humphrey and Williamson, 2001).

Major salivary glands: The largest major glands are the human parotid glands (PG), with an average weight of 25-30 g (de Paula *et al*., 2017). The PG are located opposite to the maxillary first molars, and the submandibular and sublingual glands are found in the floor of the mouth (Humphrey and Williamson, 2001). The main excretory duct of the PG is the Stensen´s duct, which enters the oral cavity in the buccal mucosa, after crossing the masseter muscle and penetrating through the buccinator muscle. The parotid glands are formed by serous acini and produces aqueous saliva (de Paula *et al*., 2017).

The submandibular glands represent the second largest pair of salivary glands with the weight from 7 to 15 g. The main excretory duct of the submandibular glands, the Wharton´s duct, opens at each side into the oral cavity under the tongue by the lingual frenum at a structure called the sublingual caruncle. Submandibular glands are composed of mixed acini with most serous and fewer mucous saliva secreting cells (Holmberg and Hoffman, 2014).

The human sublingual glands represent the smallest group of salivary glands with an average weight of approximately 3 g. They are located between the connective tissue of the mouth and the mylohyoid muscle (de Paula *et al*., 2017).

The sublingual glands have small ducts called Rivinus and Bartholin´s duct, which connect with Wharton´s duct at the sublingual caruncle (Holmberg and Hoffman, 2014). The sublingual glands are composed also of mixed acini, mucous and serous, but with a majority of mucous acinar cells and rarely found serous acini (de Paula *et al*. 2017).

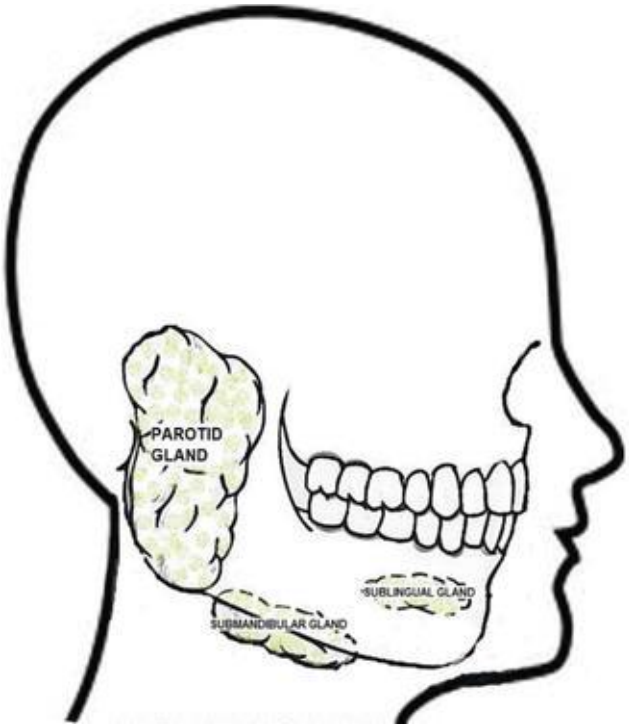

Figure 4. Locations of major salivary glands (Punj, 2018)

In a healthy adult the major salivary glands produce over 90% of saliva. The major salivary glands are highly vascularized and innervated. The transverse facial artery emerges from the superficial temporal artery to provide blood supply to the PG and traverses along Stensen´s duct. The facial artery, a branch of the external carotid artery, brings blood supply to the submandibular glands (SMG) and passes through the gland capsule before crossing the inferior border of the mandible (Holmberg and Hoffman, 2014).

1.1.3. Salivary composition and production

Saliva is a very valuable oral fluid that is critical to the preservation of oral tissues and maintenance of oral health. Saliva makes major contributions as the initial interface to our environment and diet (Arnold and Ribeiro, 2019). It contains countless components such as enzymes, mucinous substances, antibacterial components etc. Saliva is a multi-functional fluid, which maintain the oral cavity in the physiological state, owing to its lubricating, buffering, taste, bone/teeth formation, antibacterial and immune properties by acting as a physiological barrier to infections (Punj, 2018). Salivary secretion is therefore critical for oral function and health (de Paula *et al*., 2017).

Saliva is a complex mix of fluids from major and minor salivary glands and from gingival crevicular fluid. Saliva is composed of more than 99% water and also includes a variety of other components as shown in table 1.

Table 1. Components of saliva: (mg/100 mL) (Kumar *et al*., 2017)

	Resting	**Stimulated**
Organic constituents	**mean**	
Proteins	220	280
Amylase	38	
Lysozyme	22	11
IgA	19	
IgG	1.4	
Glucose	0.2	
Nitrogenous products		
Ammonia		3
Urea	20	13
Inorganic constituents		
Sodium (Na)	15	60
Potassium (K)	80	80
Calcium (Ca)	5.8	6
Magnesium (Mg)		

These components interact in related functions: (1) modulate pH in the oral cavity by buffering action and clearance capacity of saliva; (2) lubricating the hard and soft oral surface which is important for speech, mastication and swallowing; (3) salivary mucins bind to bacteria and

prevent bacterial adhesion to tooth enamel, providing antibacterial and antiviral activities; (4) lysozyme, enzyme that lyses bacterial and prevents overgrowth of oral microbial population; (5) as an antisoulubility factor modulate demineralization and remineralization (Pfaffe *et al*., 2011; Humphrey and Williamson, 2001).

The parotid glands contribute 20% of the unstimulated flow, 65% is produced by the submandibular glands, 8% from sublingual glands and less than 10 % from numerous minor glands (Humphrey and Williamson, 2001). Through stimulation, the parotid glands contribute more than 50 % of total salivary secretion, where sublingual glands contribute to a small percentage, as in the unstimulated state of salivary gland. The average daily flow of whole saliva varies between 0.5 and 1.5 L saliva, depending on the references. The unstimulated flow rate is approximately 0.3 to 0.4 mL/min, which decreases by 0.1 mL/min by sleep, and increases to about 4 to 5 mL/min during eating and other stimulating activities (Iorgulescu, 2009).

The formation of saliva occurs in two stages. The first stage involves the formation of saliva by the serous or mucous acinar cells. Serous cells produce serous saliva, which is thin, aqueous and contains more proteins, while mucous cells produce thick, viscous saliva containing mucopolysaccharides and mucin.

In the second stage, saliva passes through the salivary ductal system, which is formed of different types of ducts (intercalated, striated and excretory ducts). Saliva secreted from acini is isotonic or slightly hypertonic when it reaches the first structure (intercalated ducts), which is then conveyed to the striated ducts, where electrolytic exchanges (reabsorption of sodium and chloride as compared to the secretion of potassium), which makes saliva hypotonic. As the saliva turns more hypotonic, the excretory duct secretes the saliva into the oral cavity (de Paula *et al.,* 2017; Punj, 2018).

1.2. Salivary biomarkers

A biomarker definition is recently established by the U.S. Food and Drug Administration and the National Institute of Health as a part of their joint Biomarkers, EndpointS, and other Tools (BEST) resource. A biomarker is defined as a characteristic that is measured as an indicator of normal biological processes, pathogenic processes or responses to an exposure or intervention (Califf, 2018).

Clinical biomarkers, for example, include pulse rate, blood pressure, fever, clinical biochemistry, and complex laboratory tests of blood, and other tissues. Biomarkers have been used in clinical medicine for decades, and hold promise for early diagnosis and effective treatment of several diseases (Ahsan, 2018). Biomarkers exist in a variety of different forms, including genetic material (e.g., DNA, RNA), proteins, lipids, antibodies or microbes. Changes in their structure, function, concentration and action can be associated with the progression or regression of a particular disorder or how the body is responding to it. Understanding and evaluating a biomarker can be useful in determining the presence, location and even likelihood of disease. Biomarkers serve as a valuable tool in the detection, risk assessment, diagnosis, prognosis and monitoring of diseases (Yoshizawa *et al*., 2013). In clinical care, monitoring biomarkers may be measured during one or more periods of a patients clinical monitoring, and measurements may sometimes detect signs of disease or condition worsening, which may indicate deteriorating prognosis or a need for intervention. Biomarker monitoring can also determine how a drug is metabolized by a patient by monitoring drug concentration, to detect therapeutic effects or disease progression while on or following treatment or to detect toxicity (FDA-NIH Biomarker Working Group, 2016).

1.2.1 Ferritin and C-reactive protein as a potential salivary biomarker

Ferritin

Ferritin is present in most tissues as a cytosolic protein and plays an important role in the storage of intracellular iron and releases it in a controlled fashion required for cellular proliferation and metabolic renewal (Jagannathan *et al.,* 2012). Ferritin is a spherical protein composed of 24-subunits of two types, the ferritin H chain (FHC), heavy type (~ 21 kDa) and ferritin L chain (FLC), light type (~ 19 kDa) (Li *et al*., 2009). In humans, H refers to ferritin isolated from the human heart, rich in the heavier (H) subunit, and L refers to ferritin from the human liver, which is rich in the lighter subunit (Wang *et al*., 2010). The ratio of FHC and FLC within ferritin varies from species to species and from organ to organ, and can be modified as response to inflammation (Li *et al*., 2009).

Serum ferritin is known as a marker for iron deficiency anemia and is used to indicate the state and severity of various diseases. Ferritin levels seem to reflect the magnitude of iron stores in the body, and decreased or increased serum ferritin levels are used as a marker for anemia and iron overload disorders. However, it involves drawing of venous blood and carries more risk of contamination. Assessment of the iron status has proven to be difficult, especially in children living in areas with high infection pressure (Jagannathan *et al*., 2012). This led to the development of a less invasive method for assessment of ferritin with the same sensitivity and specificity levels as ferritin assessment of blood.

As ferritin appears in saliva, salivary ferritin could represent an alternative diagnostic marker for disease detection in the future. Jagannathan and co-workers observed that ferritin levels in saliva were much higher (153.24 ±26.58 µg/dL) than the serum levels (31.69 ±6.28 µg/dL) in patients with severe iron deficiency anemia. The mechanism by which anemia cause a rise in salivary ferritin is not exactly known. It may be speculated that ferritin probably is important for the iron dependent enzymatic functions of the saliva, but it also helps in the conservation of iron through saliva or ferritin is increasingly endocytosed by the ducts of salivary glands and extracted into the saliva (Jagannathan *et al*., 2012).

The results of studies that have been accomplished to study the relation of serum and saliva ferritin levels are different. Increased ferritin concentration in saliva has been observed by Agarwal and co-workers in a study on children with anemia with iron deficiency (Agarwal *et al*., 1984).

However, a concrete transport mechanism of ferritin from blood to saliva is still not examined. Studies have shown that ferritin can function as effective iron carrier and can be taken up via human transferrin receptor (TfR) to provide iron to cells (Wang, *et al.,* 2010). TfR is a membrane glycoprotein, which is distributed on the endothelial cells surface at the apical side (Khan, Liu & Dutta, 2018).

TfR is regulated by iron response elements-binding proteins (IRP1 and IRP2), depending on the iron concentration. There are two types of TfR, TfR-1 and TfR-2, which differ in their binding affinity and cell type expression. *Li et al.* (2010) reported that TfR-1 functions as an important cell-surface receptor for heavy ferritin (HFt), with almost no binding to light ferritin (LFt) in activated blood lymphocytes and circulating reticulocytes (Li *et al*., 2010).

C-reactive protein (CRP)

Inflammation, cardiovascular disease, viral and bacterial infections, tissue injury, stress and other diseases are associated with elevated serum levels of C-reactive protein (CRP). For example, viral infections or mild inflammation led to a serum CRP level between 10 and 40 mg/L, whereas bacterial infections and trauma causes serum levels to be greater than 300 mg/L (Pay and Shaw, 2019).

The presence of CRP in saliva provides an opportunity for development of non-invasive assessments of diseases risk (Dillon *et al*., 2010). CRP is one of several plasma proteins, which is predominantly synthesized by the liver and is used as blood marker. CRP is a pentameric 125.5 kD positive acute phase protein (APP) that is believed to be a part of the innate immunity and recognizes molecular patterns found on cells undergoing apoptosis as well as found on the surface of pathogens (Pay and Shaw, 2019).

CRP is secreted by hepatocytes under the transcriptional control of the cytokine IL-6 (Ouellet-Morin, Danese, Williams, Arseneault, 2011), and induces the production of matrix metalloproteinases and tissue factor expression in monocytes (Mahajan, Bahl, Dhawan, 2010). Because of its non-lipophilic structure and high molecular weight, CRP is likely to show limited transfer from blood to saliva (Ouellet-Morin, Danese, Williams, Arseneault, 2011).

Recently, CRP has been shown to regulate the expression of receptor for advanced glycation end-products (RAGE) in endothelial progenitor cells (EPCs) (Chen, *et al*., 2009). RAGE is a member of the immunoglobulin superfamily of cell surface molecules. It interacts with a wide

range of ligands including advanced glycation end products, modified low density lipoproteins, amyloid fibrils and various S100 proteins (Mahajan, Bahl, Dhawan, 2010). RAGE is a multi-ligand receptor expressed by many cell types. Ligands of this receptors activate RAGE leading to oxidative stress, propagation of inflammatory response and vascular dysfunction (Chen *et al.,* 2012; Bierhaus *et al*., 2005).

RAGE was initially isolated from bovine lung, vascular endothelial and smooth muscle cells (Chen *et al.,* 2012). Recent studies suggested that RAGE may play an important role, especially for diabetic patients, in promoting inflammatory processes and endothelial activations, which accelerate coronary atherosclerotic development (Zhong *et al.,* 2006).

Ferritin, CRP and other parameters are commonly measured through venipuncture, which is an invasive procedure and requires skilled professionals, laboratory equipment and considerable financial resources. In contrast, saliva collection is a non-invasive, stress-and pain-free method. This procedure provides an important advantage in comparison to blood tests being easily available and non-invasive.

1.3. Transport across biological barriers

The blood-saliva barrier (BSB) is defined as epithelia of oral cavity and salivary glands. In addition to epithelial cells, other cell types infiltrate the oral mucosa, such as Langerhans cells, melanocytes, Merkel cells or endothelial cells forming blood vessels that might contribute to barrier functionality (Bierbaumer *et al.,* 2018).

A major goal of recent studies was the *in vitro* modelling of epithelia of the oral and salivary glands because standardized models are lacking for oral cavity or salivary glands epithelia. Furthermore, the epithelia of different regions in the oral cavity show significantly different barrier properties, as well as epithelia from salivary glands. Only a small number of the studies using BSB *in vitro*-models are dealing with transport processes of molecules (Bierbaumer *et al*., 2018).

1.3.1. Epithelial barriers

Epithelial barriers are found in many tissues such as the intestine, kidney and brain where they separate the external environment from the body or a specific compartment from its periphery. To cross an epithelial barrier, a molecule or element must reach the epithelial barrier cells, get across, and be exported on the other side. The epithelial barrier cells are connected with tight junctions that help to establish the apical and basolateral side of the membrane (van Meer and Simons, 1986).

The apical and basolateral compartments face completely different environments and the epithelial cells are able to sense the two environments. Nutrients and other molecules are transported across the barrier. The direction of transport is dictated in part by the expression of transporters and receptors on the respective membrane. For example, Transferrin receptor (TfR) has been used extensively as a marker for recycling-endosome trafficking and its localization defines the transport direction.

1.3.2. Transfer of biomolecules from blood to saliva and *vice versa*

Transporters are membrane-bound proteins that mediate the translocation of substrates across biological membranes (Lin *et al*., 2015). Most of the organic compounds in saliva are produced in the salivary glands, but some molecules pass into saliva from blood. Several pathways, both intra- and extracellular, enable molecules to be transported from blood to saliva (Pfaffe *et al.,* 2011).

Passive diffusion carrier-mediated diffusion, active transport, endocytosis can be routes for the absorption *via* the salivary glands (Figure 5). Passive diffusion is possible *via* intracellular gaps (paracellular) or *via* the cell membrane (transcellular) (Lauffler, 2014).

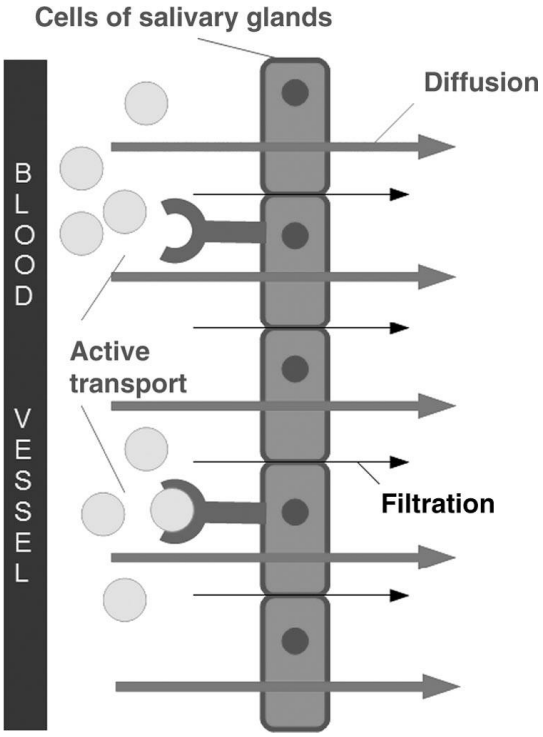

Figure 5. Schematic representation of the transportation of biomolecules from blood into saliva (Pfaffe *et al.*, 2011).

Paracellular permeability across epithelial cells is largely regulated by intercellular junctions known as the tight junction (TJ) (Bruewer and Nusrat, 2006). The tight junctions and adherens junctions (AJs) are often referred to as the constituents of the apical junctional complex (AJC), because they are more tightly associated and residue at the apical end (Zihni *et al.,* 2016).

The AJC is composed of a multiprotein complex. Tight junctions form selectively permeable barriers between two distinct compartments, and they are dynamically regulated to control paracellular ion transport and solutes based on their molecular size and charge (Bruewer and Nusrat, 2006).

In addition to tight and adherens junctions, epithelial and some other types of cells are bound tightly by desmosomes. These are buttonlike points of contact between cells, often thought of as a “spot-weld” between adjacent plasma membranes, that confer mechanical strength on these tissues (Lodish, Berk, Zipursky *et al.,* 2000).

Main membrane protein components found in tight junctions are occludin, claudins and tricellulin. The C-terminal domain of occludin is bound to one of a group of actin associating

proteins (zonula occludens 1-3 (ZO 1-3)), that are linked to other cytoskeletal proteins (Lodish, Berk, Zipursky *et al*., 2000).

The junctional complex of epithelial cells consists of three components: tight junctions (TJ), adherens junctions (AJ) and desmosomes and is located at the most-apical part of the lateral membrane. In epithelial cellular sheets, adherens junction and desmosomes mechanically link adjacent cells, and TJs are responsible for intercellular sealing. Tight junctions act as paracellular gates that restrict diffusion of ions and solutes based on their molecular size and charge (Tsukita, Furuse and Itoh, 2001; Zihni *et al.,*2016). The main protein components important for the structure of TJs are tetraspan proteins of the claudin family (consisting of over 20 different members) and the three junctional domain proteins: junctional adhesion molecules (JAMs), occludin and tricellulin (Zihni *et al.*, 2016).

As the first component of tight junctions was identified a peripheral membrane protein ZO-1(zonula occludens-1) with a molecular mass of 220 kDa. The TJs contains also other adaptor proteins, many of which interact with each other, forming a protein network. For example, ZO-2 and ZO-3, two proteins that co-immunoprecipitate with ZO-1 (Tsukita, Furuse and Itoh, 2001).

Adherens junctions (AJs) are cell-cell adhesion complexes. The prominent AJs is the zonula adherens, found in most epithelial cells. Zonula adherens links the cells into a continuous sheet and separate the apical from basolateral membranes. AJs includes interactions of the cadherin family, such as E-cadherin and the catenin family members p120-catenin, β and α-catenin. Together they control the formation, maintenance and function of AJs (Hartsock and Nelson, 2008).

Desmosomes are another type of cell junctions that provide strong adhesion between cells. They also link intracellularly to the intermediate filament cytoskeleton, and they form adhesive bonds in a network that gives mechanical strength to tissues. Desmosomes are formed of desmoglein and desmocollin proteins (Garrod and Chidgey, 2007).

The topmost additional and specialized layer, the stratum corneum, contributes to the paracellular barrier of the stratified parts of the oral mucosa. Lamellar bodies also called membrane coating granules are formed and released by keratinizing epithelial cells during the differentiation process and contain lipids (e.g., glucosylceramides), hydrolytic enzymes and proteins (e.g., corneodesmosin). These components are released after the secretion of the

granules and spread over the cell surfaces supporting the formation of a thick cell envelope which is water-impermeable and resistant against keratinolytic agents. It is a strong shield preventing paracellular permeability in keratinized stratified squamous epithelia of the oral mucosa. However, in non-stratified epithelial layers TJ might form the major paracellular barrier (Bierbaumer *et al.*, 2018).

In salivary glands, TJs allow unidirectional saliva secretion and maintain a cellular barrier between blood and tissues fluids (Baker, 2010). The expression of tight junction (TJ) proteins in salivary and *in vitro* models is mostly investigated at the mRNA or protein level by PCR or Western blot analysis (Bierbaumer *et al*.,2018).

Active transport

A second pathway for the entry of molecules into saliva is active transport through the secretory cells of the glands (Figure 5) (Pfaffe *et al.,* 2011). During recent years, two major superfamilies of membrane transporters have been extensively studied, namely ATP-binding cassette (ABC) and solute carrier (SLC) transporters. The human family of ABC transporters contains 49 members (Li *et al*., 2012). A bit less than 400 SLC membrane transporters have been annotated in the human genome (ITC, Giacomini, Huang, Tweedie *et al.,* 2010).

Expression of both transporter families has been detected in barrier forming epithelia of major organs such as kidney, liver, intestine, placenta and eye, as well as organs with barrier functions, such as brain (Lin *et al*., 2015). Both transport families act differently. ABC importers appear to be restricted to prokaryotes, ABC exporters are found in all living organisms and are responsible for the active efflux of a wide range of different molecules such as hydrophobic drugs, lipids, peptides and even proteins including toxins such as hemolysin (Seeger and Van Veen, 2008). In most examples, transport of the substrates against their concentration and chemical potential gradients is driven by the hydrolysis of ATP (Li *et al*., 2012). ABC transport system contain two nucleotide-binding domains (NBDs) where ATP is bound and hydrolyzed, also named the ATP binding cassettes domains and two membrane domains (MDs), which mediate transport of substrates across the cell membranes (Seeger and Van Veen, 2008).

In contrast, solute carrier (SLC) members are primarily involved in the uptake of small molecules into cells, that do not rely on ATP hydrolysis (Lin *et al.,* 2015). ABC and SLC transporters have been described to be polyspecific, i.e., to transport several substrates with different affinities

and regulations in district tissues (Bierbaumer *et al.,* 2018). Much is still unknown about SLC transporters, partly because the study of SLC transporters can be hindered using in vitro models, as many cell lines that have undergone multiples passages lose transporter expression and activity (Lin *et al.,* 2015).

Current data suggest that active transport across buccal mucosa seems to be rare. In this context, Lin *et al.* showed expression of ABC transporters (*P*-glycoprotein) in TR146 cells. The established TR146 model could be used to test the role of this ABC transporter on the pharmacokinetics of oral drugs and biomarkers. *P*-gp was described to actively transport the steroid hormone cortisol, a biomarker often used to evaluate the stress level of patients (Lin *et al.,* 2020a).

Endocytosis

Endocytosis is a diverse set of processes used by the cell to internalize specialized regions of the plasma membrane as well as small amounts of extracellular fluid (Apodaca, 2001). Endocytosis is fundamental in the regulation of cell metabolism, signal transduction, differentiation, defense and motility (Ivanov, Nusrat and Parkos, 2005) and the prerequisite for the transcytosis process across biological barrier. To internalize molecules from the extracellular space, cargo material is engulfed by an invagination of the plasma membrane. Two main types of endocytosis are classified depending on the size of ingested material (Bierbaumer *et al*., 2018). By phagocytosis, the ingestion of larger particles such as microorganisms is accomplished, on the contrary, pinocytosis is the process for the uptake of fluids and small particles. Endocytosis could be mediated via receptors or adsorption on the cell membrane. The transferrin receptor (TfR) is a receptor relevant for endocytosis at the oral epithelium. TfR is primarily distributed on the basolateral surface in differentiated cells, which presents an obstacle for receptor mediated endocytosis (Du, Fan, Zheng *et al.,* 2012).

Some strategies for oral drug delivery, were based on receptor-mediated endocytosis, for example, nanocarriers such as nanoparticles, lined with transferrin aimed at binding to the transferrin receptor and to enhance the cellular uptake and transport of orally administrated drug via transferrin receptor mediated endocytosis into epithelial cells (Du, Fan, Zheng *et al*., 2012).

2. AIM

Over the past years, saliva has gained increasing attention as a diagnostic fluid. Saliva offers advantage over serum because it can be collected noninvasively, and there is a minimal risk of causing infections during saliva collection. Saliva can also be used in clinically challenging situations, such as obtaining samples from children, anxious or handicapped patients or from the elderly, from whom blood sampling could be a difficult task.

The aim of the proposed master thesis is to examine the validity of salivary ferritin and CRP as a non-invasive biomarker by trying to understand the relationship between salivary and blood levels of these two biomarkers using two *in vitro* models of the BSB. Transport studies of ferritin and CRP should be accomplished across the human buccal mucosa carcinoma cell line TR146 as an oral mucosa model and human submandibular cell line HTB-41(clone B2) as salivary gland model.

After the elucidation of a possible present preferred transport direction (apical to basolateral or basolateral to apical) first investigations about the possible involvement and regulation of TfR for ferritin transport and RAGE for CRP transport should be conducted. In case that an active transport for one of these biomarkers could be found across models of the BSB a causal link between blood and saliva levels could be assumed.

3. Material and Methods

3.1. Materials

3.1.1. Cell Lines

Cell line TR146

The human buccal oral mucosa cell line TR14 was commercially acquired from Sigma-Aldrich (10032305). The human cell line TR146 originates from a neck node metastasis of buccal carcinoma and has become a standard model. TR146 cells can form multilayers of squamous stratified epithelia with approximately 4-7 cell layers and an average thickness of 40 µm after 3 weeks of culture (Bierbaumer *et al*.,2018). The buccal oral mucosa cell line TR146 was cultivated in Dulbecco´s Modified Eagle Medium (DMEM, Sigma-Aldrich, D5796), supplemented with 1% Penicillin/Streptomycin (Pen/Strep, Merck, A2213) and 10 % FCS (Fetal Calf Serum, Sigma-Aldrich, F9665) at 37°C, 5% CO2, 95% air atmosphere and 95% humidity.

Cell line HTB-41 (clone B2)

The submandibular salivary gland cell line HTB-41, first isolated and described by Giard *et al.* (1973) was commercially acquired from the company ATCC (30-2007). The isolated clone B2 from human submandibular cell line HTB-41 (Lin *et al.,* 2020 (b)) was cultivated in McCoy´s 5A media (Life technologies, 16600-082) supplemented with 1% Penicillin/Streptomycin (Pen/Strep, Merck, A2213) and 10% FCS (Fetal Calf Serum, Sigma-Aldrich, F9665), termed as McCoy media.

3.1.2.Cell Culture Material

Table 2. List of materials used for cell cultures

Dulbecco´s Modified Eagle´s Medium (DMEM) –high glucose; 500 mL	Sigma-Aldrich; D5796
Dulbecco´s Phosphate Buffered Saline Solution (DPBS) 1x	Gibco, Ref: 14190-094
Trypsin/EDTA solution; 0.05%/ 0.02 %	Millipore; L2143
Penicillin/ Streptomycin 10.000 units (P/S)	Merck; A2213
Fetal Calf Serum (FCS)	Sigma-Aldrich; F9665
Human Keratinocytes Growth Supplements (HKGS)	Thermo Fisher Scientific; S0015
Hank´s Balanced Salt Solution (HBSS)	Sigma-Aldrich; H6648
McCoy´s 5A Medium (1x)	Thermo Fisher Scientific; 16600082
Cell culture flasks (T25)	Greiner,Bio-One GmbH, CELLSTAR®, 690175
Cell culture 24-well plate	Greiner, Bio-One GmbH; CellStar; 662160
Thincert cell culture insert for 24-well plates	Greiner Bio-One GmbH, 662641
Cell culture 6-well plate	Greiner, Bio-One GmbH, 657160
Thincert cell culture insert for 6-well plates	Greiner, Bio-One GmbH, 657641
Tube 15 mL	Falcon ®; 353502
Tube 50 mL	Sarstedt; 62.559.001
Serological pipettes 5 mL	Sarstedt; 86.1253.001
Serological pipettes 10 mL	Sarstedt; 86.1254.001
Serological pipettes 25 mL	Sarstedt; 86.1685. 001
Syringe 3 mL	BD; Luer-Lok™ Tip; 309658
Syringe 10 mL	BD; Luer-Lok™ Tip; 300912
Syringe 30 mL	BD; Luer-Lok™ Tip; 301229
Sterican® needle	Braun; BD; 9161627S
Sterile syringe Filter, PVDF	Carl ROTH, SE2M229I04
Pipette tips 10 µL	Biozym; SafeSeal SurPhob VT0200
Pipette tips 100 µL	Biozym; SafeSeal SurPhob VT0230
Pipette tips 200 µL	Biozym; SafeSeal SurPhob VT0240
Pipette tips 1250 µL	Biozym; SafeSeal SurPhob VT0270
Petri dishes	Greiner Bio-One; 633181
Eppendorf tubes 1.5 mL	Eppendorf; 0030 120.086

3.1.3.Chemicals and Substances

Table 3. List of used chemicals and substances

ß-Mercaptoethanol	Sigma, M3148
RA1 bufferfrom NucleoSpin-Kit	Machery-Nagel, 740961
Pierce™ BCA Protein Assay	Thermo Scientific; 23227

3.1.4. Materials for ELISA

Table 4. List of materials used for the Ferritin ELISA

96-well plate, high-binding microtiter plates	Greiner Bio-One GmbH; 655094
NaCl; Mw: 58.44 g/mol	Sigma-Aldrich; S7653-250G
KCl; Mw: 74.55 g/mol; EMSURE®	Merck; 1.04936.0500
Na_2HPO_4; Mw: 141.06 g/mol; EMSURE®	Merck; 1.06586.1000
KH_2PO_4; Mw: 136.08 g/mol; EMSURE®	Merck; 1.04873.1000
Bovine Serum Albumin Fraction V biotin free	Carl Roth GmbH; EG-Nr. 2923225
Supersignal ELISA Pico Chemiluminescent Substrate	Thermo Scientific; 37070
Tween® 20	Sigma-Aldrich; P7949

Table 5. Primary and secondary antibodies used for Ferritin ELISA

Ferritin Antibody (cAB); [5.15 mg/mL]	East coast Bio; HM304
Native Human Ferritin Protein; [3 mg/mL]	Aviva Systems Biology; NP_000137.2
HRP Antibody (F31); [1.1 mg/ml]	NovusBio; NB110-8385H

Table 6. List of materials used for the CRP ELISA

High binding 96 well plate	Corning 3366 Costar Assay plate; 3366
Non-binding 96 well plate	Corning 3461 Assay plate; 3461
Substrate solution: 1-step ultra TMB-ELISA	Thermo Scientific; 34028
EDTA disodium salt, dihydrate;	Merck; 324503
Bovine Serum Albumin (BSA)	Sigma- Aldrich; A7906-100G
NaCl; Mw: 58.44 g/mol	Sigma-Aldrich; S7653-250G
KCl; Mw: 74.55 g/mol; EMSURE®	Merck; 1.04936.0500
Na_2HPO_4; Mw: 141.06 g/mol; EMSURE®	Merck; 1.06586.1000
KH_2PO_4; Mw: 136.08 g/mol; EMSURE®	Merck; 1.04873.1000
Carbonate-bicarbonate buffer	Sigma-Aldrich; C3041
HCl 1M	Roth; 6792.1

Table 7. Primary and secondary antibodies used for C - reactive protein ELISA

Human C-reactive Protein/CRP kit:	**R&D Systems; DY1707**
Capture Human CRP Antibody	R&D Systems; 842676
Human CRP Standard Antibody	R&D Systems; 842678
Human CRP Detection Antibody	R&D Systems; 842677
Streptavidin-HRP	R&D Systems; 890803
Human RAGE	**R& D Systems; 1145-RG**

3.1.5. Devices

Table 8. List of used devices

Biosafety cabinet (BSC)	Thermo Scientific, HERAsafe KS 18
Incubator	Thermo Scientific, HERAcell VIOS 1601
Water bath	Grant, SUB Aqua Pro
Pipettes 10 µL, 100µL, 200µL, 1000µL	Eppendorf, research plus
Multichannel pipettes 300 µL	Eppendorf, research plus
Multichannel pipettes 200 µL	VWR, Ergonomic High-Performance
Pipette boy	Sartorius, midi plus
Thoma cell counting chamber	Optik Labor, “Neubauerimproved”, 1100000
Microscope (brightfield)	Olympus, GKX41
TEER-measurement, Millicell® ERS-1 Voltammeter	Merck, MERS00001
TEER-measurement, chopstick electrode	WPI, STX2
Enspire® 2300 Multimode Plate Reader	PerkinElmer, Waltham, MA, US
Shaker	Roth, mini gyro-rocker SSM3
Megafuge 40R Centrifuge	HRRAEUS, Thermo Scientific
T3000 Thermocycler	BIOMETRA
Light Cycler 480 II	Roche, Basel, Switzerland

3.1.6. Materials for real-time quantitative PCR

Table 9. List of used materials

RNAse Away Reagent	Invitrogen by Thermo F. Scientific; 10328-011
RNA Isolation kit, NucleoSpin® RNA	Macherey-Nagel, 740955.250
High-Capacity cDNA Reverse Transcription kit	Applied Biosystems by Thermo F. Scientific; 4374966
MultiScribe™ Reverse Transcriptase	Applied Biosystems by Thermo F. Scientific; 4311235
Power Up SYBR Green	Appliedbiosystems by Thermo F. Scientific; A25742
RNAse Inhibitor	Applied Biosystems by Thermo F. Scientific; N8080119
Nuclease free Water (NF H_2O)	Ambion The RNA Company, AM9937
FrameStar® 96 Well Semi-Skirted PCR Plate; Roche Style	4 titude; 4ti-0951
Syringe 1mL	Braun, Omnican 40; 9161627S
Thermo Cooler	Biozym, 733350

Table 10. Primer sequence of applied markers for qPCR

Primer	Forward 5´-3´	Reverse 5´-3´	Identification
18sRNA	ATGGTTCCTTTGGTCGCTCG	GAGCTCACCGGGTTGGTTTT	NM_003286.2
TfR	AGCCCACTGTTGTATACGCT	TTTCTCAACTTTGCTGGCCC	NM_0013139966.1 NM_001313965.1 NM_003234.3 NM_001128148.2
PPIA	GTTCTTCGACATTGCCGTCG	TGAAGTCACCACCCTGACAC	NM_021130.4
RAGE	GAAGCTTGGAAGGTCCTGTCTC	CCGGAAAATCCCCTCATCCTG	NM_001136.5 NM_001206929.1 NM_001206936.1 NM_001206966.1

Used Software for the quantification was Light Cycler® 480 V1.5 software (Roche, Basel, Swicherland).

3.2. Methods

The blood-saliva barrier (BSB) *in vitro models* used in this master thesis are composed of culture set-ups using the Transwell system. To investigate the transport of ferritin across the blood-saliva barrier, the human cell line TR146, originating from a neck node metastasis of buccal mucosa was used as a standard model representing the oral mucosa, whereby the human cell line HTB-41 (B2 clone) was used as a model for the salivary gland (Lin *et al*., 2020). Barrier properties of the models were assessed by TEER (transepithelial electrical resistance) measurements. Transport of ferritin and CRP across these models was measured by ELISA (Enzyme-linked Immunosorbent Assay). Different transport study designs such as apical to basolateral and basolateral to apical at different concentrations of the biomarkers were performed as well as transepithelial electrical resistance (TEER) measurement to assess the barrier function of TR146 cell and HTB-41 (clone B2) cells.

3.2.1. Seeding and cultivation of TR146 cell line on Transwell inserts

All working steps with cell material was carried out under sterile conditions using sterile disposable or autoclaved material. The human buccal carcinoma cell line TR146 was cultured in T25 flasks (Greiner Bio-One, CELLSTAR®, 690175) in Dulbecco´s Modified Eagle´s Medium (DMEM, Sigma-Aldrich, D5796) with 10% Fetal Calf Serum (FCS, Sigma-Aldrich, F9665) an 1% Penicillin/Streptomycin (Pen/Strep), abbreviated as DMEM media, and incubated at 37°C in 95% humidified atmosphere containing 5% CO_2. Media change was performed every 2-3 days and cell were propagated weekly at a cell concentration of $9.33*10^3/cm^2$.

Table 11. Media used for TR146 cell line cultivation in T25 flasks and for 24-well plate

	Media	Substance	Percentage	mL
T25 flask	DMEM media (DMEM++)	DMEM, high glucose	100%	500
		FCS (fetal calf serum)	10%	50
		Penicilin/Streptamicin	1%	5
24-well plate	DMEM media with HKGS (DMEM++, HKGS)	DMEM, high glucose	100%	500
		FCS (fetal calf serum)	10%	50
		Penicilin/Streptamicin	1%	5
		HKGS	1%	5

For transport studies, the cells were seeded in 24-well inserts (Greiner Bio-One; ThinCerts ™ 662641) at a cell density of $4.8*10^4/cm^2$ in 300 µL DMEM media, and with 900 µL DMEM media provided on the basolateral compartment in 24-well plates (Greiner Bio-One, 662160). For this, medium was aspirated from the T25 flask, then the cell surface was washed twice with 5 mL DPBS (Dulbecco´s Phosphate-buffered saline). Cells were detached with 0.7 mL 0.05%Trypsin/ 0.02 % EDTA solution (Merck, L2143) and incubated for 5 minutes at 37°C (5% CO_2). After the incubation cells were seeded with a cell density $4.8*10^4$ cells/cm^2 for 24 well plate and $2.33*10^5$ for T25 flask. In the 24-well plate, 8 inserts were used as a blank, and the other 16 inserts contained the TR146 cell line (Figure 6).

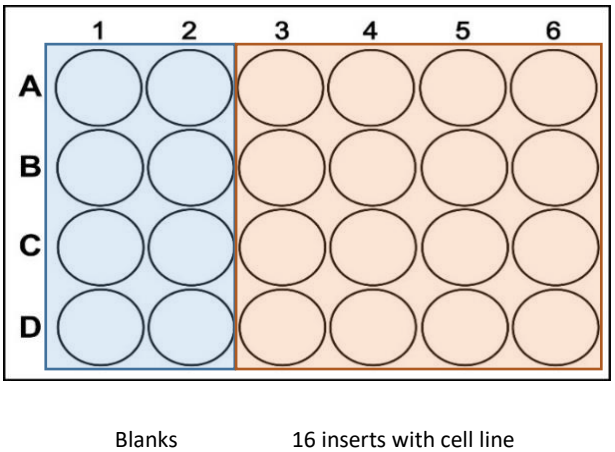

Figure 6. Scheme of the prepared 24-well plate for ferritin transport studies

3.2.2. Seeding and cultivation of HTB-41 (clone B2) cell line on Transwell inserts

The isolated clone B2 from the human submandibular cell line HTB-41 was cultured in T25 flasks. The cells were kept in McCoy´s 5A Medium (Life technologies, 16600082) with 10% Fetal Calf Serum (FCS) and 1% Penicillin/Streptomycin (Pen/Strep), termed as McCoy media, and incubated at 37°C in 95% humidified atmosphere containing 5% CO_2. The cells were splitted weekly at a cell density of $8*10^4$ cells/cm^2 or seeded also at a density of $8*10^4/cm^2$ on 24-well inserts (Greiner Bio-One; Thin Certs ^{TM} 662641). On the 24-well plate, the cells were seeded as previously described in 3.2.1. 300 µL McCoy media were added on the apical side of the inserts, and 900 µL media was filled in the basolateral side for culture one inserts. Media change was performed every 2-3 days until the day of experiment on day 15 or 16.

First medium change of the Transwell model was performed two days after seeding with the same medium (DMEM media for TR146 cell line or McCoy media for clone B2). The inserts were checked under the microscope for contaminations.

For changing the medium, the apical media of the inserts was discarded using tweezers in a petri dish and inserts transferred to a new empty 24 well plate (washing plate). Medium from the first plate was checked again under the microscope and aspirated after that. New media was added (900 µL medium per well), inserts were transferred back, and fresh 300 µL of the medium was filled into the apical side of the inserts to maintain cultivation under submerged condition.

The change of the medium continued every 2^{nd}-3^{rd} day with media. As soon as cells become confluent on day 5 or 8, the cultivation condition was switched from submerged to airlift, and basolateral DMEM media was changed to DMEM media supplemented with 1% Human Keratinocytes Growth Supplements (HKGS, Gibco, S0015) for TR146 cell line. Airlift means, that no media was added to the apical and there was only media in the basolateral compartment. For HTB-41 (clone B2) cells the 300 µL media was added to the inserts. Media change was performed every 2-3 days for four weeks until the TR146 cell line were used for the transport experiment.

3.2.3. Measurement of Transepithelial Electrical Resistance

The measurement of transepithelial electrical resistance (TEER) was carried out in the laminar air flow hood. First TEER measurement was performed on the 2nd day after seeding, after changing the media as described above for B2 clone (HTB-41 cell line), or at the experimental day for TR146 cell line. For the TEER measurement medium was also added to the inserts after ALI (Air Liquid Interface) cultivation of TR146 cells.

The plate was equilibrated to room temperature (RT) in the laminar for 30-40 min. In the meantime, 15 mL tube were prepared with about 7 mL 70% sterile EtOH and with 7 mL medium. The chopstick electrode (WPI, STX2) was first disinfected for maximum 5 minutes with 70% EtOH and calibrated for 10 minutes in the growth medium. After equilibrium time TEER was measured. The inserts had to be arranged in the middle of each well, because the position of the electrode could significantly influence the measurement results. The shorter electrode should not be in contact with the cell layer, while the longer electrode should just touch the bottom of the well as shown in figure 7.

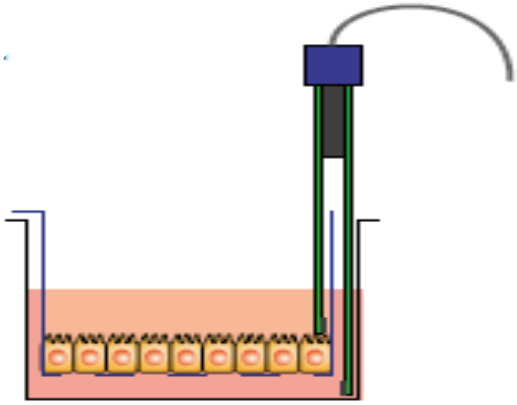

Figure 7. TEER measurement with an STX2 chopstick electrode in a Transwell system (Lea, 2015)

The inserts without cells were measured prior to inserts containing cells. After TEER measurement the plate was placed back in the incubator. TEER measurements were done every two to three days. When the maximum TEER was reached, the transport experiment was performed for B2 clone. The TEER measurement for TR146 cell line was only measured on the day of experiment since it is known that TEER will decrease with every submerging step.

To calculate the TEER value [Ω* cm^2] first the average value of the blank was subtracted from the resistance value of each sample. Afterwards the value was multiplied by the growth area of the inserts (0,336 cm^2 for 24-well inserts).

$$TEER\ [\ \Omega * cm^2] = (\ value\ [\Omega] - mean\ of\ blanks\ [\Omega]) * growth\ area\ [cm^2]$$

3.2.4. Transport Experiments

3.2.4.1. Ferritin Transport Experiments across TR146 cell layers

After 30 days of culture the insert grown TR146 cells were used for transport experiments with ferritin. As the cells grew under airlift conditions, the conditions were changed to submerged for TEER measurement. The inserts were checked under the microscope and media was replaced with fresh DMEM media supplemented with 1% HKGS: 900 µL of media in the basolateral and 300µL in the apical side. After TEER measurement in DMEM media supplemented with 1 % HKGS the apical media of the inserts was discarded in a petri dish and inserts were transferred to a washing 24-well plate (Greiner Bio-One; 662160) which contained HBSS in the wells.

The cell layers of TR146 were washed twice on the apical side (300 µL) with HBSS and transferred to the measurement plate with 900 µL HBSS, after which 300 µL HBSS was added. The plate was again incubated for 30-40 minutes at room temperature. The plate of the culture with basolateral DMEM media supplemented with 1% HKGS was stored in the incubator at 37°C until the second day and used for TEER measurement after 24-hour sampling. During the 30 minutes incubation time, the electrode was sterilized again in 70% EtOH for 5 minutes and calibrated in HBSS for 10 minutes. After TEER measurement HBSS was discarded into a petri dish, remaining HBSS was aspirated carefully using a micropipette.

For the transport experiment human ferritin (Aviva Systems Biology, San Diego, CA, USA; OPSA10506) was then applied at a concentration of 300 ng/mL or 1000 ng/mL in the respective salt solution (HBSS)-by exchange of the total apical (A) or basolateral (B) medium for transport studies from apical to basolateral (A/B) compartment or from the basolateral to apical (B/A) compartment. The plate scheme is shown in figure 8.

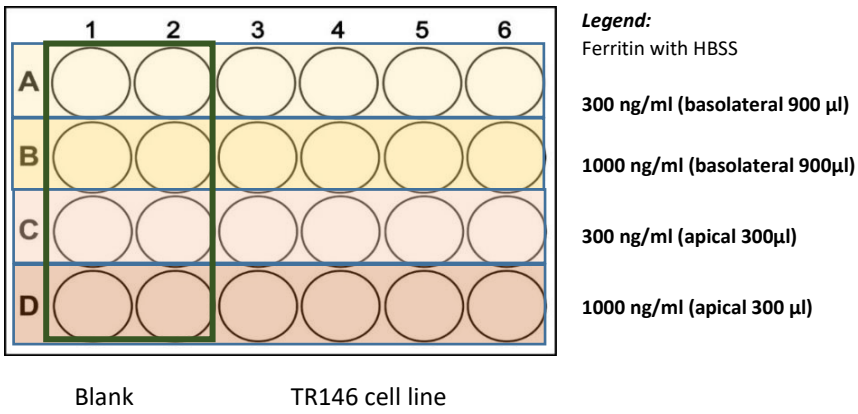

Figure 8. Scheme of the prepared 24-well plate with TR146 cells for Ferritin transport experiment at two different directions

After incubation for 24 hours at 37°C in the incubator, samples from the apical and basolateral side were collected and stored at -20°C until analysis with ELISA. After the sampling, the inserts were transferred to the measurement plate used previously to measure TEER in HBSS and subsequently in DMEM ++ HKGS as described above. After two TEER measurements cells from two 24-well inserts from the same treatment were lysed with 350 µL lysis buffer (RA1 Buffer (Machery-Nagel,740961) supplemented with 1% ß-Mercaptoethanol) and pooled as one sample and stored at -80°C until RNA isolation.

3.2.4.2. Ferritin Transport Experiments across HTB-41 (clone B2) cell layers

After two weeks of cultivation with TEER measurement every 2-3 days, the filter grown B2 clone (HTB-41 cell line) were used for ferritin transport experiments. The cell layers on 24-well inserts were checked under the microscope and media was replaced with fresh McCoy media, as described above (3.2.2.). The cells in 24-well inserts were equilibrated at room temperature for at least 30 minutes prior to transepithelial electrical resistance (TEER) measurement. In the meantime, the electrode was sterilized for maximum 5 minutes in 70% sterile EtOH and calibrated in media for 10 minutes. New 24-well plate was also prepared with McCoy media (without FCS) supplemented with 1% Pen/Strep for subsequent measurement. After TEER measurement the apical media of the inserts were discarded in a petri dish and inserts were transferred to washing 24-well plate (Greiner Bio-One; 662160), washed twice on the apical and basolateral side with 300 µL or 900 µL McCoy media (without FCS).

TEER was subsequently measured in McCoy media. Apical media was discarded in petri dishes and the residues were carefully removed using a micropipette.

The plate with the basolateral McCoy media (McCoy media with FCS) was stored in the incubator at 37°C until the second day and used for TEER measurement after 24-hour sampling. For the transport experiments human ferritin (Aviva Systems Biology, San Diego, CA, USA; OPSA10506) was applied at a concentration of 300 ng/mL or 1000 ng/mL in the respective McCoy media supplemented with 1% Pen/Strep (without FCS) -by exchange of the total apical (A) or basolateral (B) medium for transport studies from apical to basolateral (A/B) compartment or from the basolateral to apical (B/A) compartment (Figure 9).

.

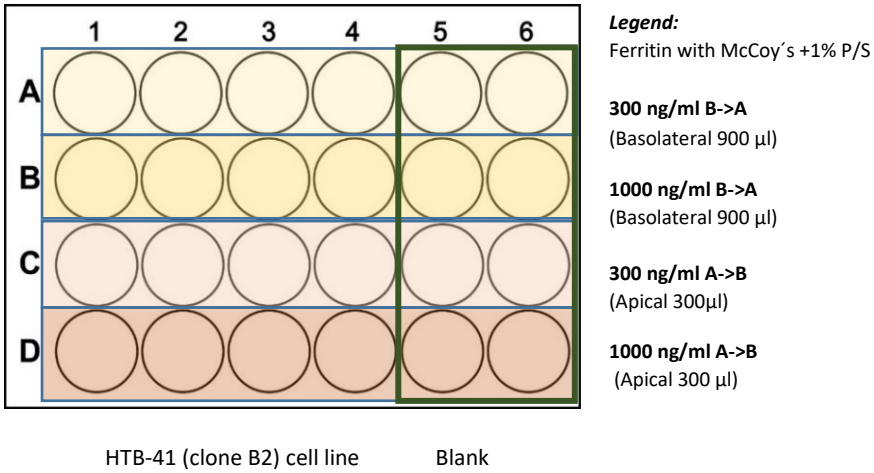

Figure 9. Scheme of prepared 24-well plate with HTB-41 (clone B2) cells for Ferritin transport at two different directions

After incubation for 24 hours at 37°C samples from the apical and basolateral side were collected and stored at -20°C until analysis with ELISA. The inserts were transferred to the measurement plate containing McCoy media for TEER measurement as described above. After the TEER measurements, two inserts treated with the same concentration and direction were lysed with 350 µL lysis buffer for RNA lysis pooled as one sample and stored at -80°C until RNA isolation.

3.2.4.3. C-reactive protein Transport Experiments with HTB-41 (clone B2) cell line

After two weeks of cultivation the filter grown B2 clone cells were used for CRP transport experiment. Before the transport study with CRP, TEER measurements were performed as described before. First TEER measurement was performed with McCoy media supplemented with 1% Pen/Strep and 10 % FCS and after two washing steps with serum free McCoy medium, TEER was measured with serum-free McCoy medium supplemented with 1% Pen/Strep.

For the transport experiment, human CRP (Sigma-Aldrich, C4063, 1 mg/mL in 20mM Tris containing 280 mM NaCl) was diluted 1:100 to 10 µg/mL CRP in McCoy media containing 1% 20 mM Tris (Roth, 5429.3, 20 mM) and 280 mM NaCl (Sigma-Aldrich, S7653), and was applied for transport studies from apical to basolateral (A/B) compartment or from the basolateral to apical (B/A) compartment (Figure 10), and incubated for 24 hours.

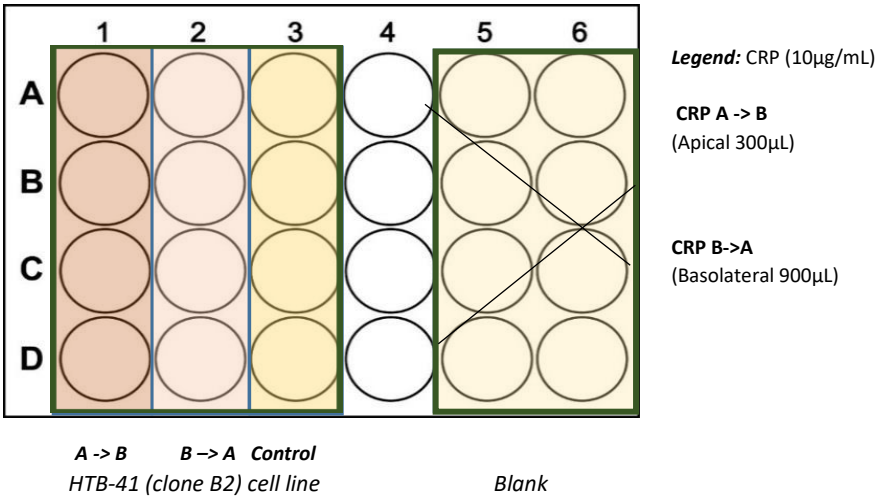

Figure 10. Scheme of prepared 24-well plate with HTB-41 (clone B2) cells with CRP [10 µg/mL] at two transport directions

The samples of the apical and basolateral side were collected after 24 hours and stored at 4°C until quantification with ELISA. After the sampling, the inserts were transferred to the measurement plate prepared previously with McCoy media supplemented with 1% Pen/Strep for TEER measurement as described above. Similarly, to the described procedure in 3.2.3. TEER was measured in McCoy media containing 1% Pen/Strep and 10% FCS, subsequently. RNA samples were collected by lysing two inserts pooling to one sample with 350 µL lysis buffer (RA1 buffer containing 1 % ß-Mercaptoethanol). Prior to RNA isolation, RNA lysates were stored at -80°C.

3.2.4.4. Effects of soluble RAGE addition on C-reactive protein transport across TR146 cell layers

After four weeks cultivation the filter grown TR146 cells were used for transport experiments with C-reactive protein (CRP) and the soluble Receptor for Advanced Glycation end products (sRAGE, R&D, 1145-RG). Similarly, to the described procedure in section 3.2.3. TEER was measured in DMEM media supplemented with HKGS and subsequently in Hank´s Balanced Salt Solution (HBSS).

For the transport experiment a CRP solution with the concentration of 10 µg/mL in the respective HBSS medium containing 1% 20 mM Tris and 5 % PBS was prepared, as well as a CRP solution with 5 µg/mL sRAGE in the respective medium. Scheme is shown below (Figure 11), cells were incubated for 24 hours at 37°C, 5% CO_2 and 95% humidity.

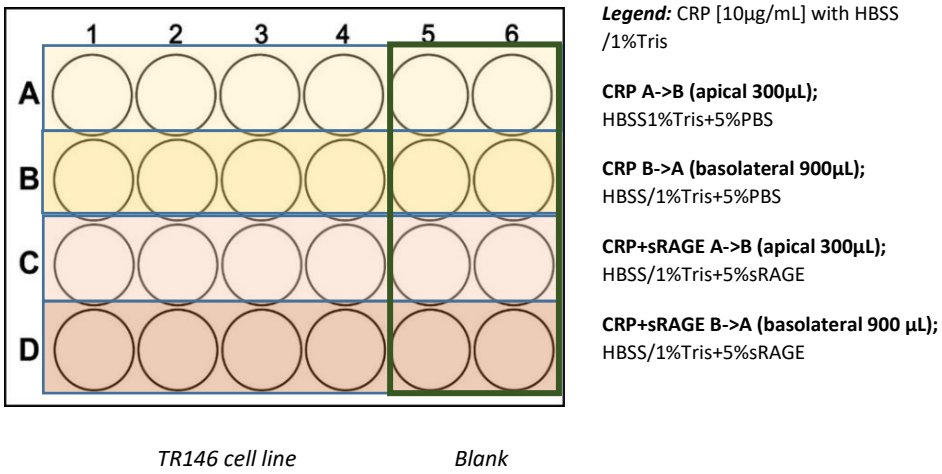

Figure 11. Scheme of prepared 24-well plate with TR146 cells; CRP and CRP with soluble RAGE concentrations for two different transport directions

The samples were collected after 24 hours, and stored at 4 °C. After sampling the inserts were transferred to the measurement plate prepared previously with HBSS, 1% 20 mM Tris and 5% PBS for TEER measurement as described above. Similarly, to the described procedure in section 3.2.3., TEER was measured in DMEM media with HKGS after the experiment.

RNA samples were collected by lysing two inserts pooled to one sample with 350 µL lysis buffer (RA 1 buffer containing 1 % ß-Mercaptoethanol). Prior to RNA isolation, RNA lysates were stored at -80°C.

3.2.4.5. Effects of soluble RAGE addition on C-reactive protein transport across HTB-41 (clone B2) cell layers

To study the influence of the soluble receptor for advanced glycation end products (sRAGE, R&D, 1145-RG) on CRP transport, 5 µg/mL sRAGE was applied together with 10 µg/mL CRP for transport studies. sRAGE was dissolved in PBS to 100 µg/mL and subsequently diluted 1:20 in McCoy media containing 1 % 20 mM Tris (Roth, 5429.3, 20mM), 5% PBS and 10 µg/mL CRP shortly before the experiment. The filter grown B2 clone cells were monitored for two weeks until a distinct paracellular barrier was reached, evaluated by TEER measurements. Prior to the start of the experiment, TEER was measured in McCoy media and after washing twice with McCoy medium supplemented with 1 % Pen/Strep, TEER was subsequently also measured in McCoy media (+ 1 % Pen/Strep) as described above in section 3.2.3.

For the transport experiment a CRP solution with the concentration of 10 µg/mL was prepared in the respective McCoy medium containing 1 % 20 mM Tris, 5% PBS (without FCS), as well as 10 µg/mL CRP with 5µg/mL soluble Receptor for Advanced Glycation Endproducts (sRAGE) in the respective medium (McCoy with 1% Pen/Strep, 1% 20 mM Tris) and was applied in a new 24 insert plate according to the scheme shown in figure 12 either on the apical (A) or basolateral (B) side for a transport from apical to the basolateral (A/B) or basolateral to apical (B/A) side. Cells were incubated at 37°C, 5% CO_2 and 95% humidity for 24 hours.

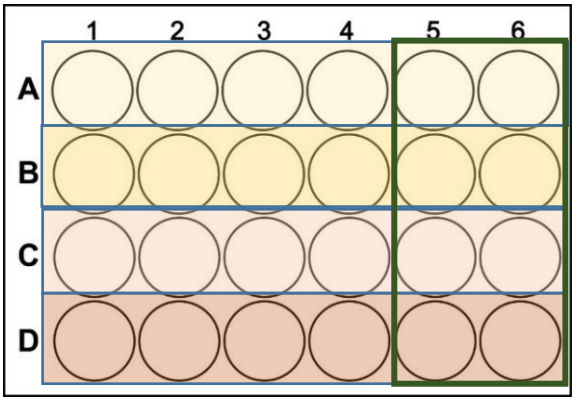

Legend: CRP [10µg/mL] with McCoy´s +1%P/S/1%Tris

CRP A->B (apical 300µL); McCoy´s+/1%Tris+5%PBS

CRP B->A (basolateral 900µL); McCoy´s+/1%Tris+5%PBS

CRP+sRAGE A->B (apical 300µL); McCoy´s+/1%Tris+5%sRAGE

CRP+sRAGE B->A (basolateral 900 µL); McCoy´s+/1%Tris+5%sRAGE

HTB-41 (clone B2) cell line *Blank*

Figure 12. Scheme of prepared 24-well plate with HTB-41 (clone B2) cells; CRP and CRP with soluble RAGE concentrations for two different transport directions

The samples were collected after 24 hours and stored at 4°C until measurement with ELISA. After sampling the inserts were transferred to the measurement plates with prepared McCoy media containing 1% Pen/Strep, 1% 20 mM Tris and 5% PBS for TEER measurement performed as previously described. After the measurement, the inserts were transferred to the McCoy media measurement plate used prior for the TEER measurement. In the end of the experiment, two inserts from the same treatment were lysed and pooled to as one sample for RNA analysis with 350 µL RA1 buffer (containing 1% ß-Mercaptoethanol) and stored at -80 °C until RNA isolation.

3.2.5. Enzyme-linked immunosorbent assay

3.2.5.1. Ferritin ELISA Assay

Enzyme-linked Immunosorbent Assay (ELISA) was done to quantify ferritin concentrations after the transport studies. For analysis of ferritin with ELISA, high-binding microtiter 96-well plates (Greiner Bio-One GmbH, 655094) were coated with 100 µL per well of 2 µg/mL ferritin coating antibody (East Coast Bio; HM304) in PBS overnight at 4°C under orbital shaking conditions sealed with aluminum foil.

Table 12. Preparation of PBS solution pH 7.3

chemicals	*Molecular weight [g/mol]*	*Concentration [g/L]*
137 mM NaCl	58.44 g/mol	8.01 g
2.7 mM KCl	74.5513 g/mol	0.2 g
8.1 mM Na2HPO4	141.96 g/mol	1.15 g
1.5 mM KH2PO4	136.086 g/mol	0.2 g

Table 13. Preparation of BSA-buffer (blocking/washing/sample-buffer)

Solutions/ reagents	*Quantity*
PBS pH 7.3	500 mL
1% Albumin biotin free	5 g (5000 mg)
0.1 % Tween 20	0.5 g

On the next day, the plate was washed three times with 300 µL per well washing buffer (PBS containing 1% bovine serum albumin (BSA; Carl Roth, 0163,2), 1% Tween 20 (Sigma-Aldrich, P7949). After the washing step, 300 µL BSA-buffer (Table 13) was added to each well and incubated for 1.5 hours at room temperature (RT) under orbital shaking conditions. A washing step with 300 µL BSA washing buffer per well was performed immediately after the incubation.

The samples with stock solution of the apical and basolateral compartment as well as used stock concentration of ferritin were additionally diluted 1:100 in HBSS or in McCoy media prior to analysis by ELISA. The standard curve with ferritin was freshly prepared as a threefold dilution series (0, 0.03, 0.1, 0.3, 1, 3, 10, 30, 100, 300, 1000 ng/mL) in BSA buffer, shown in the table below (Table 14).

Table 14. Standard curve used for Ferritin ELISA

Concentration	***Dilution***	
[ng/ mL]	***Sample [µL]***	***BSA-buffer [µL]***
1000	Stock form Transport study	
300	300 µL	700 µL
100	200 µL	400 µL
30	300 µL	700 µL
10	200 µL	400 µL
3	300 µL	700 µL
1	200 µL	400 µL
0.3	300 µL	700 µL
0.1	200 µL	400 µL
0.03	90 µL	210 µL
0	/	300 µL

After blocking with blocking buffer, the 96-well plate was washed once with washing buffer (Table 12), then 100 µL of samples and calibration curve solutions were added to the plate per well and incubated at room temperature on the shaker for 1 hour. After the incubation, the wells were washed again with 300 µL washing buffer three times and 100 µL of 100 ng/mL of detection antibody (HRP Antibody (F31) [1.1mg/mL]) NovusBio; NB110-8385H) diluted in PBS was added to each well. The plate was incubated at room temperature under orbital shaking conditions for 1 hour. After the incubation, the wells were washed with 300 µL washing buffer for three times. For the measurement 100 µL SuperSignal™ ELISA Pico Substrate (Thermo Fisher, 37070) consisting of 50:50 Super Signal ELISA Pico Lumina/Enhancer Solution and SuperSignal ELISA Pico Stable Peroxide Solution, was added per well, and the plate was sealed with aluminum foil and incubated in the dark at room temperature for 15 minutes. The measurement at of the chemiluminescent signal was done at 450 nm with the EnSpire® 2300 Multimode Plate Reader (PerkinElmer, Waltham, MA, USA).

3.2.5.2. C-Reactive Protein ELISA Assay

The human C-Reactive Protein (CRP) ELISA was carried out to quantify CRP concentration from transport study samples.

Table 15. Preparation of PBS solution pH 7,3

chemicals	*Molecular weight [g/mol]*	*Concentration [g/L]*
137 mM NaCl	58.44 g/mol	8.01 g
2.7 mM KCl	74.5513 g/mol	0.2 g
8.1 mM Na2HPO4	141.96 g/mol	1.15 g
1.5 mM KH2PO4	136.086 g/mol	0.2 g

Table 16. Preparation of buffers

Buffers	*Chemicals*	*Quantity*
Washing buffer	PBS solution pH7.3	500 mL
	0.05% Tween 20	0.275 g
Reagent diluent (RD)	PBS solution, pH 7.3	100 mL
	1% Bovine Serum Albumin (BSA)	1 g
Blocking buffer	Distilled water	100 mL
	1% Bovine Serum Albumin (BSA)	1 g
	Carbonate-bicarbonate buffer	1 capsule
100 mM EDTA	Reagent diluent (RD)	10 mL
	EDTA disodium salt	0.3722 g

The first step for the CRP ELISA was to dilute the human CRP capture antibody (R&D Systems, 842676) from the CRP kit (R&D Systems, DY1707) in PBS to a concentration of 720 µg/mL (the diluted capture antibody was aliquoted to 40 µL and stored in the freezer at -20°C.) To apply a concentration of 2 µg/mL of the capture antibody, the prepared solution was diluted 1:360 in PBS (Table 15). 100 µL per well of the diluted CRP capture antibody solution was reversely pipetted on a 96-well plate, sealed with aluminum foil overnight at 4°C under orbital shaking conditions. On the next day each well was washed with 300 µL PBS containing 0,05% Tween 20 (Sigma-Aldrich, P7949) for three times, blocked with 300 µL per well with blocking buffer (Table 16) and incubated for 1.5 h at room temperature under orbital shaking conditions sealed with

aluminum foil. Samples from the transport studies of the receiving compartment were diluted 1:25 and CRP stock solution (10 µg/mL), the stock solution and samples with stock solution were diluted 1:16 000 in McCoy media with 1% Pen/Strep and 1% Tris, and blanks were diluted 1:200 (table 18). For calibration curve the stock was first prepared from 10 µg/mL to 100 ng/mL (table 17). From the solution of 100 ng/mL calibration curve was prepared (0, 0.5, 1, 1.25, 2.5, 5, 10, 20 ng/mL) showed in table 17.

Table 17. Solution for the calibration curve used for CRP ELISA

ng/mL	***Sample [µL]***	***McCoy´s with 1% Tris [µL]***
100	**10 µL (10 µg/mL CRP)**	**990**
ng/mL	***Sample [µL]***	***McCoy´s with 1% Tris [µL]***
20	200	800
10	500	500
5	500	500
2.5	500	500
1.25	500	500
1	600	150
0.5	300	300
0		300

Table 18. Sample dilutions

CRP stock solution [10 µg/mL] and samples containing CRP stock solution		
Dilution	***Sample [µL]***	***McCoy´s +/ 1% Tris [µL]***
1:16000		
1. 1:80	12.5	987.5
2. 1:200	5	995
Samples without Stock CRP		
1:200 (blanks)	5	995
1:25	12	288

Diluted samples and the samples for the calibration curve were mixed and centrifuged as shown in table 18. 150 µL per well of 20mM EDTA (1:5 dilution of 100mM EDTA in reagent diluent) was pipetted in a non-binding 96-well plate (Corning, 3461), and 150 µL of sample dilutions was added (dilution 1:2). This was mixed and 100 µL/well of this mixture was applied as duplicates on the previously coated high binding 96-well plate. The plate was covered with an aluminum foil and incubated under orbital shaking conditions at room temperature for 1 hour.

After the incubation the plate was washed with 300 µL washing buffer containing 0,05% Tween 20 and PBS for three times, following an incubation step with 100 µL of the needed concentration of 30 ng/mL detection antibody (R&D Systems, 842677), therefor the CRP concentration of 32.4 µg/mL was diluted 1:1080 in reagent diluent (Table 16), and incubated for 1 hour at room temperature sealed with aluminum foil under shaking conditions.

After incubation the plate was washed as previously described above, and 100 µL streptavidin-HRP (R&D Systems, 890803) was diluted 1:200 in reagent diluent, and added to wells, incubated for 20 min under shaking conditions sealed with aluminum foil. After the incubation time the plate was washed again with washing buffer for three times. 1-Step™ Ultra TMB-ELISA substrate solution (Thermo Fisher Scientific, 3428) was added in volume of 100 µL per well, and the plate was incubated in the dark for 20 min at room temperature. After 20 minutes 50 µL of stop solution (1M HCL (Roth,6792,1)) was added per well and absorbance was measured at 450 nm with the EnSpire® 2300 Multimode Plate Reader (PerkinElmer,Waltham, MA USA).

3.2.6. Analysis of data

The permeated concentration of ferritin and CRP was calculated as apparent permeability coefficient P_{app} using the formula bellow, where C_{rec} is the measured concentration in the receiving chamber [ng/mL], V_{rec} is the volume of the receiving compartment [mL], time is the duration of the transport in [s], A is the surface area of the insert membrane [cm^2] and C_0 is the measured concentration of the applied stock solution [ng/mL].

$$P_{app} = \frac{C_{rec} * V_{rec}}{time * A * C_0}$$

3.2.7. RNA isolation

For RNA isolation of cell lysates, the NucleoSpin RNA Kit (Machery Nagel, 740961) was used according to the manufacturer´s instruction. The lysed cells were homogenized with a syringe (Braun, 9161627S), by pulling up and down the sample substance 10 times. After the homogenization the lysate was filtered through NucleonSpin® Filter (violet ring) for 1 min at 11000 x g (=rcf). Afterwards the filter was thrown away, 70% EtOH was added to the supernatant and transferred to a new column. For each preparation one NucleoSpin®RNA Column (light blue ring) was placed in a collection tube. The lysate was loaded to the column and centrifuged at 11000 x g for 30 seconds. The column was placed in a new collection tube (2mL), 350 µL MDB (Membrane Desalting Buffer) was added and centrifuged at 11000 x g for 1 minute to dry the membrane.

In the meantime, the DNase reaction mixture was prepared in a sterile 1.5 mL microcentrifuge tube: for each isolation, 10 µL reconstituted rDNase was added to 90 µL reaction buffer and mixed by flicking the tube. 95 µL DNase reaction mixture was applied directly onto the center of the silica membrane of the column and incubated for 15 minutes at room temperature. After the incubation, 200 µL of buffer RAW2 was added to the NucleoSpin®RNA Column, as a first wash and centrifuged at 11000 x g for 30 seconds. The buffer RAW2 inactivated the rDNAse. The column was placed into a new collection tube (2 mL), and 600 µL of buffer RA3 was added to the NucleoSpin®RNA Column, centrifuged at 11000 x g for 30 seconds.

The flow-through was discarded, placed back to the collection tube and 250 µL of buffer RA3 was added to the column, and centrifuged at 11000 x g for 2 minutes to dry the membrane completely. The column was placed into a nuclease-free collection tube (1.5 mL) and 40 µL RNase-free H_2O was added, incubated for 1minute at room temperature and centrifuged at 11000 x g for 2 minutes, to elute the RNA and stored at -80°C. The eluted RNA (RNA tube needs to be on ice), was measured with the Nanodrop 2000D, where 1 or 2 µL of eluted RNA was pipetted on the lower measurement surface of the device. The generated data was offset by computer-based software.

3.2.8. Production of cDNA

For further analysis with quantitative PCR, RNA had to be converted into complementary DNA (cDNA). Before starting the preparation of cDNA, the RNA samples were thawed on ice, vortexed and centrifuged. For cDNA synthesis with the Multiscribe Reverse Transcriptase Kit (Thermo Fisher Scientific, 4311235) master mix was prepared according to the table below (Table 19).

Table 19. Master Mix preparation for 1 reaction (RXN)

Reactive approach	***Volume[µL]***
10x RT Buffer	2
25x dNTP Mix (100mM)	0.8
10x RT Random Primers	2
Multiscripe Rev. Transcriptase	1
RNAse Inhibitor	1
Nuclease-free H2O	3.2
total volume	**10**

The final volume of one reaction was 20 µL, consisting of 10 µL master mix and a 10 µL mixture of RNA and nuclease-free water (NF-H_2O). The selected amount of RNA to be transcribed with the Multiple Reverse Transcriptase Kit (Applied Biosystem Thermo Scientific, 4311235) was 200 ng RNA for clone B2, and 1000 ng RNA was for TR146 cell line.

Depending on the RNA concentration each sample was diluted with nuclease-free water (NF-H_2O) to the final volume of 10 µL. 10 µL master mix were distributed to clearly labeled PCR tube, RNA-NF-H_2O mix was added and following RNA was then transcribed to cDNA (thermal cycler: 10 minutes at 25°C, 120 minutes at 37°C, 5 minutes at 85°C and continuously at 4°C). After reverse transcription cDNA was diluted 1:10 and stored at -20° C and the undiluted cDNA was stored at -80°C.

3.2.9. Real-time quantitative polymerase chain reaction

Real time quantitative polymerase chain reaction (RT-qPCR) is a method which is used to track the amplification of a specific mRNA target sequence during PCR.

For measuring the expression of transferrin receptor (TfR), TfR and PPIA primer sequences could be found in table 10. As endogenous control peptidylprolyl isomerase A (PPIA) was chosen. PPIA is the most constant gen that was analyzed in 78 samples including cell lines and tissues brain, breast, colon, kidney, ovary, pancreas, prostate, skin, and vascular origin.

Every experiment contained duplicates of four differently treated samples. Two samples were treated with 300 ng/mL ferritin from the apical-to basolateral side (A/B) and two samples with the same concentration from basolateral-to apical side (B/A). This scheme was repeated with a concentration of 1000 ng/mL ferritin. In addition to these treated samples, duplicates of untreated samples were tested simultaneously on every qPCR plate. The untreated samples were also isolated, cDNAs were made and diluted 1:10.

To increase the validity of the method and decrease occurred errors, samples were always tested in triplicates, as well as a triplicate of blanks, lacking cDNA, was added. A primer stock solution with a dilution of 1:33 and two separate master mixes were prepared. Each mastermix contained the PowerUp-SYBR-Mastermix, nuclease-free water (NF-H_2O) as well as the specific diluted primerpair (TfR/ PPIA), lacking the cDNA (Table 20).

Table 20. Mastermix for performing qPCR reactions

1x reaction mixture	***Volume [µL]***
PowerUp SYBR Green MM	10
Primerpair (TfR or PPIA)	2.8
Nuclease-free water (NH-H2O)	3.2
total volume	**16**

16 µL of the mastermix were dispensed into the premarked wells of a 96-well pate (4titude, Dorking, UK; 4ti-0951) following a specific scheme (Figure 14). As seen in the figure 14, the mastermix with TfR primerpairs was distributed into yellow marked wells and the mastermix with PPIA primers were distributed into blue marked wells. 4 µL of diluted cDNA (1:10) of each sample was added to their marked spot at the 96 well plate and carefully pipetted up and down when adding cDNA to the mastermix (Figure 13).

To exclude random contaminations or reagent contaminations “No-Template-Controls” also called blank were added to every plate in triplicates, consisting of the mastermix with PPIA and NF-H_20 without cDNA. The plate was covered with its specific foil, centrifuged for 20 seconds, and put into the LightCycler 480 II (Roche, Basel, Switzerland). The program for qPCR was set for 20 sec 95°C for activation, running 40 cycles for 3 s at 95°C and 30s at 60 °C, following a melting stage of 15 s at 95°C, 1 min at 60°C and 15 s at 95°C. Data was acquired with the LightCycler 480 V1.5 software. ΔCt values were calculated by subtracting Ct values of the endogenous control from the respective Ct values of the analyzed targed. ΔCt values of treated samples were normalized to untreated samples upon exponentiating by 2 as shown with the formula below and displayed as x-fold values.

$$\frac{2^{-\Delta Ct}\ treated}{2^{-\Delta Ct}\ untreated}$$

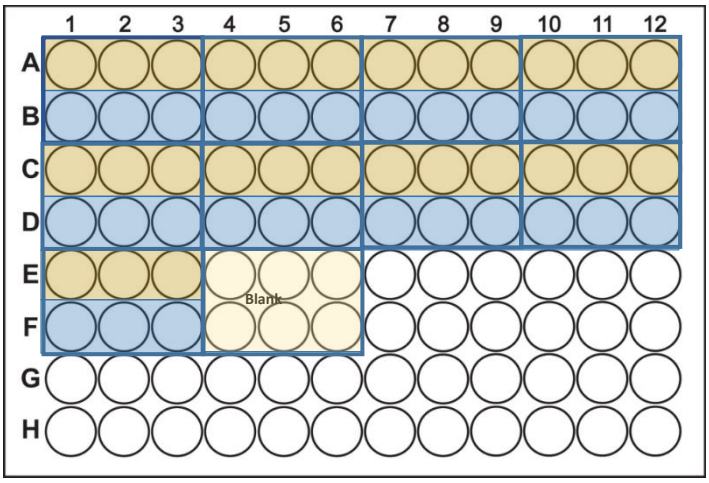

Figure 13. Pipetting schema of samples for qPCR. Yellow marked wells were filled with mastermix containing TfR primer and the blue marked wells were filled with mastermix containing PPIA primer.

3.2.10. Statistical Data Analysis

Results are shown as mean ± SEM unless otherwise indicated. Statistical analysis was performed with Student´s *t-test or two-way ANOVA* with *α=0.05, p< 0.05*, p<0.01**, p<0.001* ***.

4. Results

The primary aim of this study was to investigate the transport mechanism of diagnostic relevant molecules across the blood-saliva barrier to evaluate their potential as salivary biomarkers. For this purpose, ferritin and CRP were selected as biomarkers to be studied.

4.1. Ferritin transport studies

Before transport studies were performed with HTB-41 (clone B2), the medium for the transport studies had to be selected. For this, a toxicity assay (LDH, Roche, Cat. No. 04744926001) was performed according to the manufacturer´s instruction with medium samples collected after six and 24 hours cultured of HTB-41 (clone B2) cells incubated in McCoy´s (w/o FCS, with Pen/Strep) and compared medium samples after incubation in pure HBSS (Hank´s Balanced Salt solution) (Figure 14). After six hours incubation the toxicity values were 0,564 % for McCoy´s and 0,35% for HBSS in comparison to the lysis control (100 %). After 24 hours the values were 1% for McCoy´s and 30 % for HBSS in comparison to the lysis control. The results revealed a significant harmful effect of HBSS and no increase of released LDH via porous cell membranes of HTB-41 (clone B2) cells in McCoy´s basal media (only with Pen/Strep). Thus, it was concluded that the basal McCoy´s media can be used for the transport studies for the submandibular salivary gland model based on HTB-41 (Clone B2) cells. The applicability of HBSS for transport studies with the oral mucosa model based on TR146 cells was shown before (Lin *et al.,* 2020b).

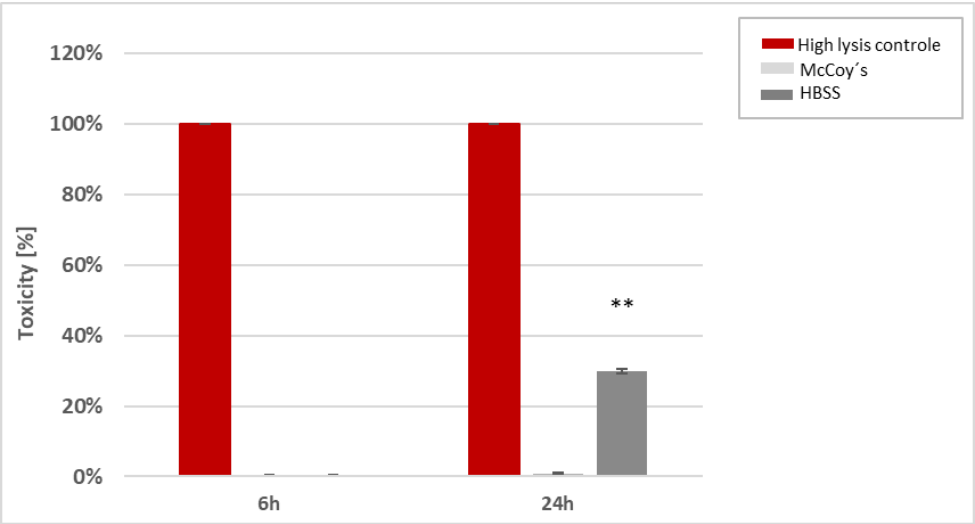

Figure 14. Results of LDH assay shown as toxicity [%] after McCoy´s basal media (w/o FCS, with Pen/Strep) and HBSS treatment for 6h and 24h. Values are shown as mean ± SD after one experiment (N=24). Statistical analysis was performed as Student´s t-test with α *=0,05;* p< 0,01 **.

4.1.1. Ferritin transport across TR146 cell layers

The apical-to basolateral (A/B) and basolateral-to apical (B/A) transport of ferritin were investigated at two different concentrations (300 ng/mL and 1000 ng/mL) in the period from 0-24 hours. Three independent ferritin transport studies with filter grown TR146 cells were performed (N=4 samples (A/B and B/A) per concentration for each experiment). Data are summarized in table 21.

Table 21. Apparent permeability coefficient P_{app} [cm/s] $*10^{-6}$ values for 300 ng/mL and 1000 ng/mL ferritin obtained in the apical to basolateral direction and basolateral to apical direction. The data are expressed as mean ± SD (standard deviation) of three independent experiments (N=2-4 per experiment). Statistical analysis was performed using Student´s t-test, α=0.05, p< 0.05*, p<0.001***.

No. Transport study (TS)	Concentration [ng/mL]	Papp [cm/s] $*10^{-6}$ A/B	Papp [cm/s] $*10^{-6}$ B/A	Student´s t-test
		mean ± SD	**mean ± SD**	**mean**
TS I	***300 ng/mL***	0,019 ± 0,002	0,029 ± 0,007	0,051
	1000 ng/mL	0,029 ± 0,010	0,027 ± 0,002	0,721
TS II	***300 ng/mL***	0,017 ± 0,003	0,033 ± 0,005	0,014
	1000 ng/mL	0,011 ± 0,002	0,022 ± 0,004	0,006
TS III	***300 ng/mL***	0,024 ± 0,009	0,053 ± 0,015	0,02
	1000 ng/mL	0,015 ± 0,009	0,024 ± 0,005	0,13
Summary TS I-III	***300 ng/mL***	**0,021 ± 0,010**	**0,038 ± 0,014**	**0,001**
	1000 ng/mL	**0,018 ± 0,011**	**0,024 ± 0,004**	**0,07**

In the first transport study, apparent permeability coefficient P_{app} in the basolateral-to apical direction (B/A) is higher compared to the apical to basolateral direction (A/B) for 300 ng/mL ferritin. While the P_{app} in the A/B direction has the same values as the B/A direction for 1000 ng/mL ferritin. In detail, P_{app} values for 300 ng/mL ferritin were 0,03 ± 0,007 $*10^{-6}$ cm/s (B/A) *versus* 0,02 ± 0,002 $*10^{-6}$ cm/s (A/B), and for 1000 ng/mL ferritin 0,03 ± 0,010 $*10^{-6}$ cm/s (A/B) *versus* 0,03 ± 0,002 $*10^{-6}$ cm/s (B/A).

In the second and third transport study, apparent permeability coefficient P_{app} shows a higher ferritin transport in the basolateral-to apical direction (B/A) for both concentrations (300 ng/mL and 1000 ng/mL), while the data show a lower ferritin transport in the apical-to basolateral direction (A/B) at both concentrations. In detail as shown in figure 16, P_{app} for 300 ng/mL ferritin in transport study II was 0, 033 ± 0,005 $*10^{-6}$ cm/s (B/A) *versus* 0,017 ± 0,003 $*10^{-6}$ cm/s (A/B)

and in transport study III was 0,053 ± 0,015 *10^{-6} cm/s (B/A) *versus* 0,024 ± 0,009 *10^{-6} cm/s (A/B).

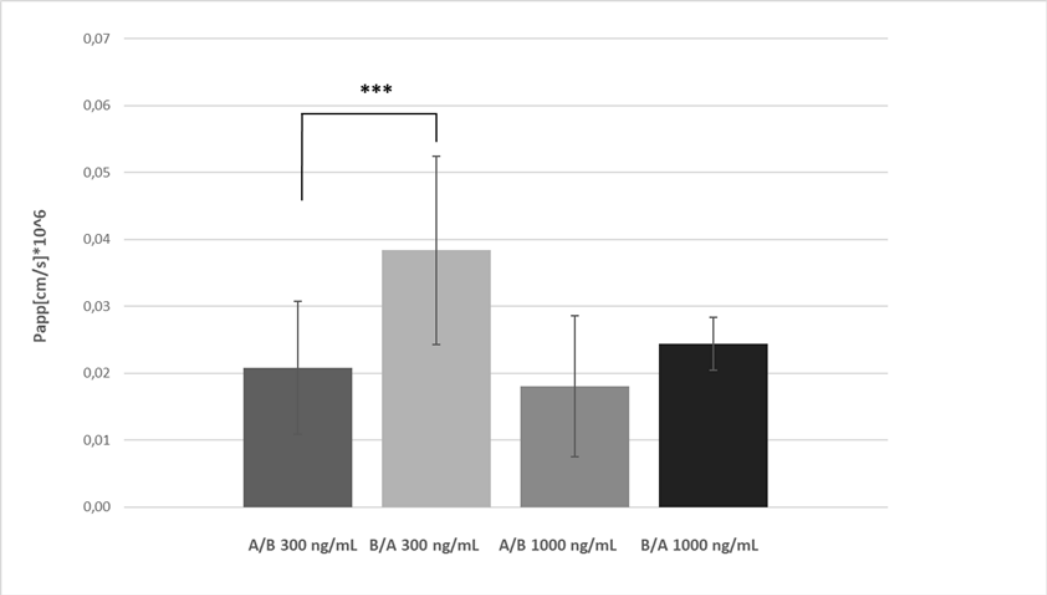

Figure 15. Apparent permeability coefficient P_{app} [cm/s] *10^{-6} for 300 ng/mL or 1000 ng/mL ferritin obtained in the apical to basolateral and basolateral to apical direction summarized for all three independent experiments (N=3, n=10-12). Data are shown as mean ± SD. Statistical analysis was performed using the student´s t-test with α=0.05, p<0.001***.

In summary, comparing the transport studies I-III, data showed a significantly increased transport of ferritin from the basolateral (blood side) to the apical (saliva) side for 300 ng/mL (Figure 15). Afterwards the ratio of B/A to A/B Papp were calculated to estimate a preferred transport direction (Table 22).

Table 22. The ratio of ferritin with two different concentrations (300 ng/mL and 1000 ng/mL) applied A/B and B/A directions on filter grown TR146 cells cultivated in HBSS. The data are expressed as mean ± SD (standard deviation) of three independent experiments (N=2-4).

Number of TS	Concentrations [ng/mL]	B/A vs A/B	
		mean	±SD
TS I	*300*	1,525	0,347
	1000	0,932	0,057
TS II	*300*	1,953	0,316
	1000	2,124	0,417
TS III	*300*	2,172	0,606
	1000	0,084	0,017
Summary TS I-III	***300***	**1,883**	**0,13**
	1000	**1,047**	**0,18**

The ratio B/A vs A/B of ferritin transport at different concentrations showed ratios between 1,525 and 2,172 in transport studies I-III at the concentration of 300 ng/mL. At the concentration of 1000 ng/mL ferritin the ratio B/A ans A/B was only increased in the transport study II (Table 22). In summary, comparing all three transport studies it can be seen that in case of 300 ng/mL there was a significantly increased transport of ferritin (p<0.01) comapring to 1000 ng/mL (Figure 16).

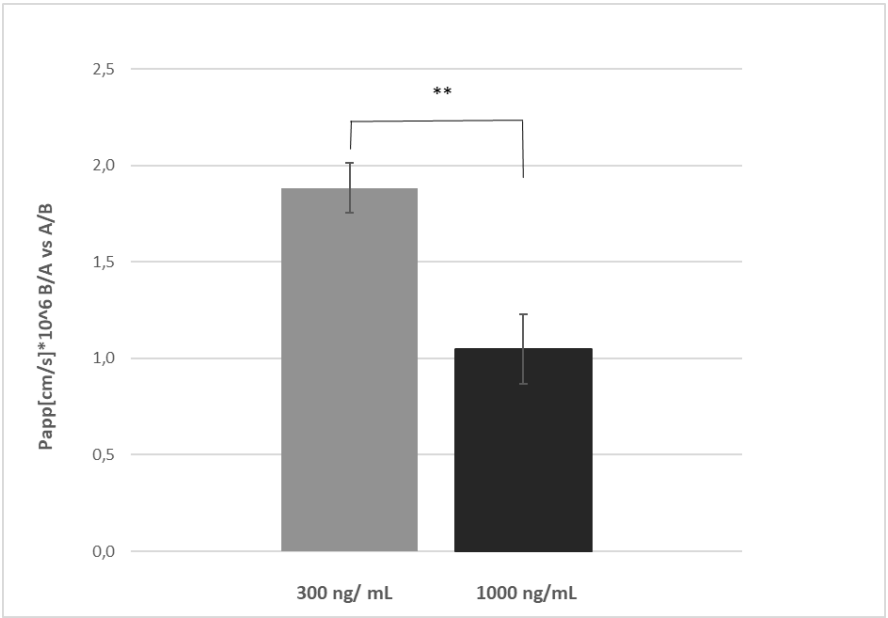

Figure 16. The ratio of two directions A/B and B/A and two different concentrations (300 ng/mL and 1000 ng/mL). Values are shown as mean ± SD for all three independent experiments (N=3, n=2-4) cultivated in HBSS. Statistical analysis was performed as Student´s t-test with α=0.05, p<0.05*, p<*0.01***.*

TR146 cell layer integrity was carefully verified by measuring the transepithelial electrical resistance (TEER) after four weeks to ensure that a confluent stratified multi-layer epithelium with distinct paracellular barrier properties was formed. To follow changes of the barrier integrity during the transport studies TEER was also measured before and at the end of the 24 hours incubation. TEER data were summarized in table 23.

Table 23. Transepithelial electrical resistance (TEER) results showed as percent for the time interval 0- 24 hours. The data are expressed as mean ± SD (standard deviation) of three independent experiments (N=2-4).

		B/A				A/B				
	HBSS without ferritin; 0h			HBSS with ferritin; 24h		HBSS without ferritin; 0h			HBSS with ferritin; 24h	
300 ng/mL Ferritin	**Ωxcm²**	**mean**	**±SD**	**mean**	**±SD**	**Ωxcm²**	**mean**	**±SD**	**mean**	**±SD**
TS I	**165,9±15,3**	**100%**	9,2%	**18%**	6,1%	**133,6±36,4**	**100%**	27,3%	**29%**	3,2%
TS II	**423,9±80,5**	**100%**	19,0%	**11%**	2,1%	**252,9±68,9**	**100%**	27,2%	**18%**	2,1%
TS III	**365,7±137,4**	**100%**	37,6%	**13%**	2,2%	**176±32,5**	**100%**	18,5%	**28%**	4,4%
1000 ng/mL Ferritin										
TS I	**113,9±32,6**	**100%**	28,6%	**34%**	3,9%	**151,3±24,5**	**100%**	16,2%	**16%**	2,6%
TS II	**280,1±93,3**	**100%**	33,3%	**18%**	3,2%	**398,7±92,8**	**100%**	23,3%	**14%**	3,3%
TS III	**186,1±18,0**	**100%**	9,7%	**29%**	3,6%	**287,5±150,4**	**100%**	52,3%	**21%**	2,4%

In table 23, TEER values showed a significant decrease relatively to the start value (zero time) by both concentrations of ferritin (300 ng/mL and 1000 ng/mL) after 24 hours incubation.

4.1.1.1. Transferrin receptor (TfR) regulation after ferritin transport studies

The following figure 17 shows the summary of the qPCR results of ferritin treated TR146 cells. Delta cycle threshold (dCt) corresponds to the difference between the Ct values of the target of interest transferrin receptor (TfR) and the reference gene (Peptidylprolyl Isomerase A-PPIA). Under the term potency an intermediate step was calculated, 2 to power of -dCt, which was then used for calculating x-fold, or also called fold change (changes of quantities between an untreated and a treated sample). The results of the qPCR analysis for each experiment were shown as mean ± standard deviation (SD).

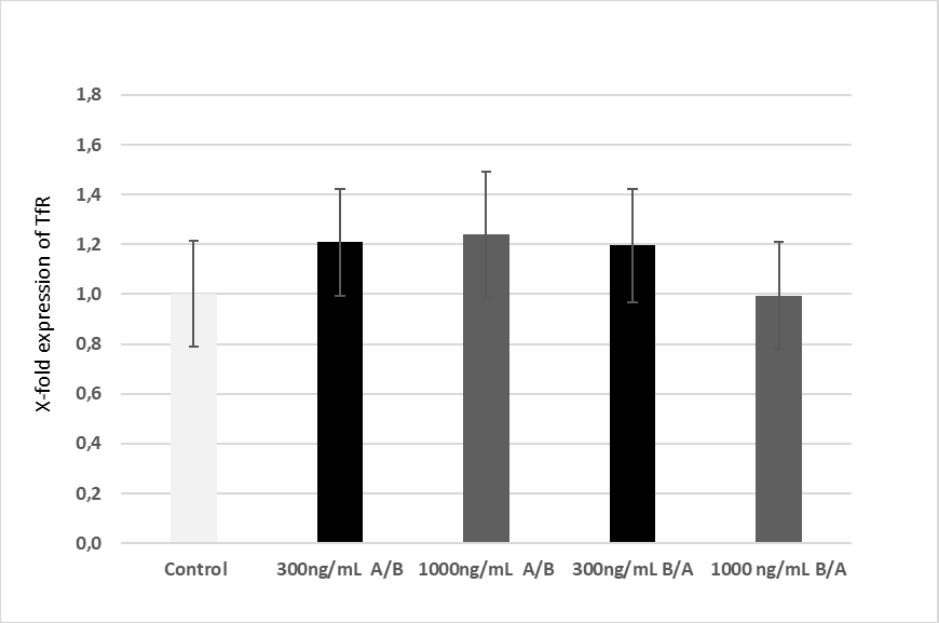

Figure 17. X-fold mRNA expression of TfR of TR146 treated with two different concentration of ferritin (300 ng/mL and 1000 ng/mL) of three independent experiments, N=8 per concentration and transport direction. Data are shown as mean ±SD.

Expression of the transferrin receptor (TfR) of ferritin treated TR146 cell line was slightly upregulated but not statistically significant in comparison to untreated control (Figure 17).

4.1.2. Ferritin transport across HTB-41 (clone B2) cell layers

Ferritin transport studies in the salivary gland epithelium model based on clone B2 were performed in three independent experiments for 300 ng/mL or 1000 ng/mL applied on the apical side (A/B) or basolateral side (B/A).

Table 24. Apparent permeability coefficient P_{app} [cm/s] $*10^{-6}$ values for 300 ng/mL and 1000 ng/mL ferritin obtained in the apical-to basolateral direction and basolateral-to apical direction. The data is expressed as means ± SD of three independent experiments (N=4). Statistical analysis was performed with student´s t-test α= 0.05, $p < 0.05$*.

No. Transport study	Concentration [ng/mL]	Papp [cm/s] $*10^{-6}$ A/B	Papp [cm/s] $*10^{-6}$ B/A	Student´s t-test
		mean ± SD	mean ± SD	mean
TS I	***300 ng/mL***	0,003 ± 0,002	0,007 ± 0,001	0,256
	1000 ng/mL	0,015 ± 0,004	0,010 ± 0,001	0,060
TS II	***300 ng/mL***	0,019 ± 0,010	0,019 ± 0,003	0,471
	1000 ng/mL	0,14 ± 0,12	0,013 ± 0,006	0,205
TS III	***300 ng/mL***	0,033 ± 0,025	0,019 ± 0,0007	0,410
	1000 ng/mL	0,016 ± 0,008	0,015 ± 0,004	0,921
Summary TS I-III	***300 ng/mL***	**0,021 ± 0,02**	**0,014 ± 0,006**	**0,335**
	1000 ng/mL	**0,015 ± 0,006**	**0,013 ± 0,004**	**0,346**

Regarding the independent experiments, the calculated apparent permeability coefficient P_{app} after 24 hours, showed a higher, but not statistically significantly higher permeation of ferritin from apical-to basolateral direction (A/B) in present of 1000 ng/mL ferritin, comparing to the ferritin transport from the basolateral-to apical direction (B/A). Comparing the concentration of 300 ng/mL ferritin per experiment, apparent permeability coefficient P_{app} is higher, but also not statistically significant, from apical-to basolateral (A/B) direction (Table 24), but in the second experiment the apparent permeability coefficient P_{app} is equal from both directions.

In detail, in first transport study (TSI), P_{app} for 300 ng/mL ferritin was 0,007 ± 0,001 $*10^{-6}$ cm/s (B/A) *versus* 0,003 ± 0,002 $*10^{-6}$ cm/s (A/B), and in second transport study (TS II), P_{app} was 0,019 ± 0,003$*10^{-6}$ cm/s (B/A) *versus* 0,019 ± 0,010 $*10^{-6}$ cm/s (A/B). For 1000 ng/mL ferritin, P_{app} was 0,015 ± 0,004 $*10^{-6}$ cm/s(A/B) *versus* 0,010 ± 0,001 $*10^{-6}$ cm/s (B/A) for first transport study (TS I), and for second transport study (TS II), P_{app} was 0,14 ± 0,12 $*10^{-6}$ cm/s (A/B) *versus* 0,013 ± 0,006 $*10^{-6}$ cm/s (B/A).

In the third experiment (TS III), the higher ferritin transport was in the apical-to basolateral (A/B) direction for both concentrations (Table 24). In summary, P_{app} for 300 ng/mL ferritin was 0,021 ±0,02 $*10^{-6}$ cm/s (A/B) *versus* 0,014 ± 0,006 $*10^{-6}$ cm/s (B/A) and for 1000 ng/mL ferritin was 0,015 ± 0,006 $*10^{-6}$ cm/s (A/B) *versus* 0,013 ± 0,004$*10^{-6}$ cm/s (B/A) (Figure 18). Afterwards the ratio of B/A to A/B Papp were calculated to estimate a prefered transport direction (Table 25, Figure 19).

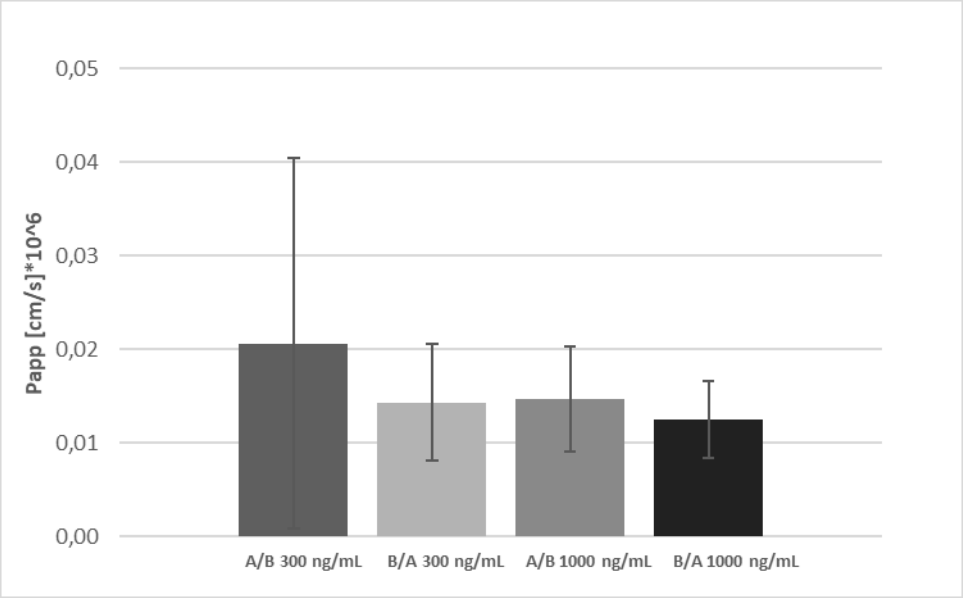

Figure 18. Apparent permeability coefficient Papp [cm/s] $*10^{-6}$ for 300 ng/mL or 1000 ng/mL ferritin obtained in the apical to basolateral and basolateral to apical direction summarized for all three independent experiments (n=3, N=8-12). Data are shown as mean ± SD. Statistical analysis was performed using the student´s t-test, with α=0.05.

Table 25. The ratio of the B/A vs A/B direction for 300 ng/mL and 1000 ng/mL applied ferritin in the salivary gland epithelium model based on clone B2. Data are displayed as mean ±SD (N=4) for all three independent experiments.

Number of TS	Concentration [ng/mL]	B/A vs A/B	
		mean	±SD
TS I	*300*	2,836	0,470
	1000	0,612	0,067
TS II	*300*	1,014	0,185
	1000	0,111	0,038
TS III	*300*	0,584	0,021
	1000	0,874	0,235
Summary TS I-III	***300***	**1,40**	**0,95**
	1000	**0,53**	**0,39**

The ratio B/A vs A/B of ferritin transport studies with two different concentrations (300 ng/mL and 1000 ng/mL), showed ratio between 0,584 and 2,836 in transport studies I-III at the concentration of 300 ng/mL, whereas the ratio at the concentration of 1000 ng/mL was below 1. Based on the results, comparing als three transport studies in the salivary gland epithelium model based on clone B2, it can be concluded that there is no active transport here either (Table 25, Figure 19). In summary, it was shown that the novel salivary gland epithelium model based on clone B2 was applicable to study the transport of the salivary biomarker ferritin.

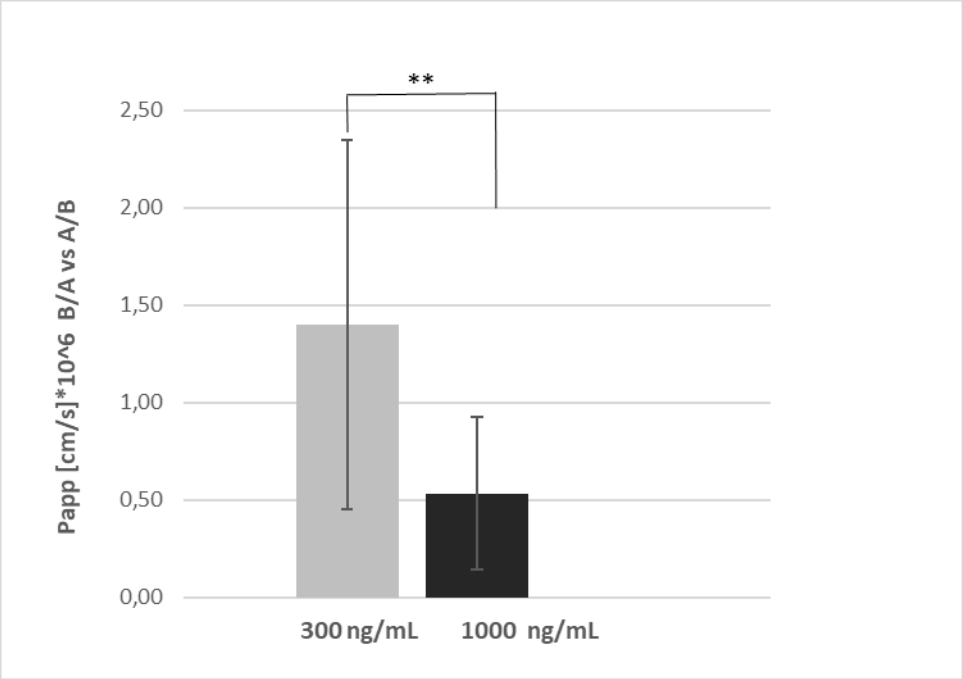

Figure 19. The ratio for 300 ng/mL and 1000 ng/mL ferritin applied on the A/B and B/A directions in the salivary gland epithelium model based on clone B2 for all three independent experiments (N=4 per experiment). Values were showed as mean ± SD. Statistical analysis was performed using the student´s t-test α=0.05, p<0.05*, p<0.001**.

HTB-41 (clone B2) cell layer integrity was carefully verified by measuring the transepithelial electrical resistance (TEER) every 2 nd - 3 rd day and after two weeks to ensure that a confluent stratified multi-layer epithelium with distinct paracellular barrier properties was formed. To follow changes of the barrier integrity during the transport studies TEER was also measured before and at the end of the 24 hours incubation. TEER data were summarized in table 26.

Table 26. Transepithelial electrical resistance (TEER) results showed as percent for the time interval 0- 24 hours. Data are shown as mean ± standard deviation (SD) for all three individual experiments (N=4 per experiment).

		B/A				A/B				
	McCoy´s +; 0h			McCoy´s+with ferritin; 24h		McCoy´s +; 0h			McCoy´s+ with ferritin; 24h	
300 ng/mL Ferritin	**Ωx cm²**	**mean**	**±SD**	**mean**	**±SD**	**Ωx cm²**	**mean**	**±SD**	**mean**	**±SD**
TS I	**275,3±46,39**	**100%**	16,85%	**9,67%**	4,69%	**419,24±31,4**	**100%**	7,49%	**6,65%**	4,51%
TS II	**292,7±107,7**	**100%**	36,79%	**4,59%**	2,61%	**567,9±213,0**	**100%**	37,50%	**2,46%**	1,13%
TS III	**344,1±56,3**	**100%**	16,36%	**8,96%**	2,28%	**561,2±115,6**	**100%**	20,60%	**6,69%**	0,57%
1000 ng/mL Ferritin										
TS I	**435,6±72,5**	**100%**	16,64%	**6,65%**	0,99%	**395,7±86,8**	**100%**	21,93%	**5,20%**	1,05%
TS II	**566,6±248,49**	**100%**	43,85%	**2,96%**	1,15%	**425,46±115,6**	**100%**	27,19%	**5,82%**	2,94%
TS III	**531,3±69,61**	**100%**	13,10%	**6,26%**	0,23%	**1311,5±152,48**	**100%**	11,63%	**2,93%**	0,50%

As can be seen from table 26 the TEER values were normalized in percentage (100%) by the value at the beginning of experiment (time zero) before adding the different concentrations of ferritin. After 24 hours ferritin treatment, TEER values showed a decrease relatively to control (zero time) by both concentrations (300 ng/mL and 1000 ng/mL).

4.1.2.1. Transferrin receptor (TfR) regulation after ferritin transport studies

The following figure 20, shows the summary of the qPCR results of ferritin treated HTB-41 cells (clone B2). Delta cycle threshold (dCt)corresponds to the difference between the Ct values of the target of interest transferrin receptor (TfR) and the reference gene (Peptidylprolyl Isomerase A-PPIA). The results of the qPCR analysis for each experiment were shown as mean ± standard deviation (SD).

We examined the expression of the transferrin receptor (TfR) upon application of ferritin and compared to untreated cells by qPCR analysis. Expression of TfR of ferritin treated HTB-41 cells (B2 clone) was significantly decreased (p< 0,0001) in both directions in comparison to untreated cells (Figure 20).

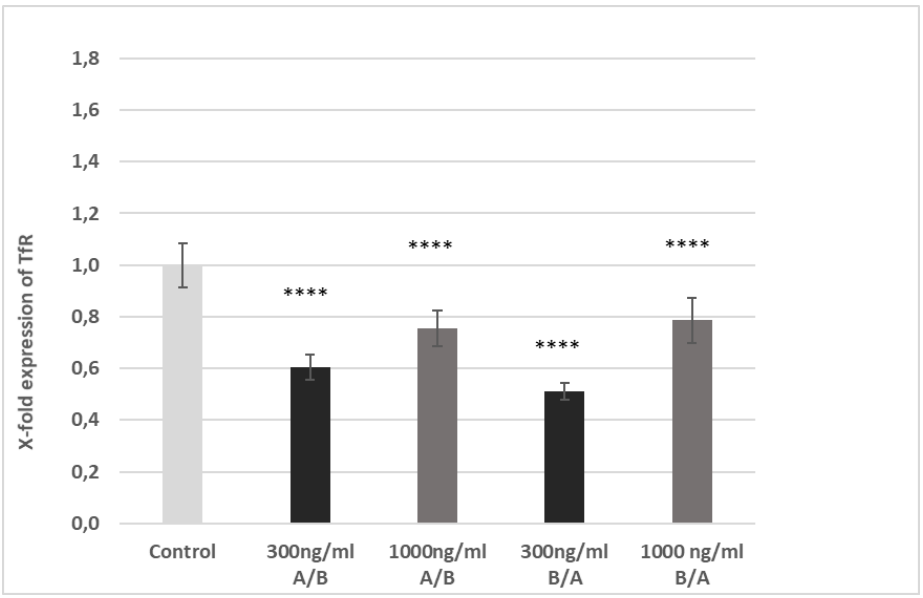

Figure 20. X-fold mRNA expression of HTB-41 (clone B2) cells treated with ferritin at two different concentrations (300 ng/mL and 1000 ng/mL) for three independent experiments (N=4 per experiment). The values are showed as mean ± SD. Statistical analysis was performed using Student´s T-test (p<0,0001****), comparing each treated to untreated/control sample.

4.2. C-reactive protein transport studies across HTB-41 (clone B2) cell layers

The optimized barrier model based on clone B2 was used to investigate the transport of C - reactive protein (CRP) across a salivary gland epithelium model. To study a possibly directed transport in detail, 10 µg/mL CRP was applied on the apical compartment (A/B) or basolateral compartment (B/A) for 24 hours in the salivary gland model. Results are summarized in table 27.

Table 27. Apparent permeability coefficient P_{app} [cm/s] $*10^{-6}$ values for 10 µg/mL C-reactive protein (CRP) obtained in the apical-to basolateral direction and basolateral-to apical direction. The data is expressed as means ± SD of three independent experiments (N=4 per experiment). Statistical analysis was performed using Student's t-test, α=0.05, p< 0.05 *

No. Transport study	**Conentration [µg/mL]**	**Papp [cm/s] $*10^{-6}$ A/B**	**Papp [cm/s] $*10^{-6}$ B/A**	**Student´s t-test**
		mean ± SD	**mean ± SD**	**mean**
TS I	**10 µg/mL**	0,013 ± 0,0008	0,019 ± 0,002	0,004
TS II	**10 µg/mL**	0,012 ± 0,003	0,04 ± 0,008	0,003
TS III	**10 µg/mL**	0,016 ± 0,003	0,03 ± 0,01	0,05
Summary TS I- III		**0,010 ± 0,005**	**0,030 ± 0,011**	**0,0002**

Regarding the independent experiments, the calculated apparent permeability coefficient P_{app} after 24 hours showed a significant increased transport of CRP from the basolateral (blood side) to the apical (saliva) side (B/A) in comparison to A/B (Table 27, Figure 21).

In summary, CRP was significantly faster from basolateral-to apical direction (B/A) in comparison to the direction apical to basolateral (A/B) (Figure 21). In table 28, as well in figure 22 the ratio of P_{app} values of B/A to A/B were listed to illustrate a possible transport directon.

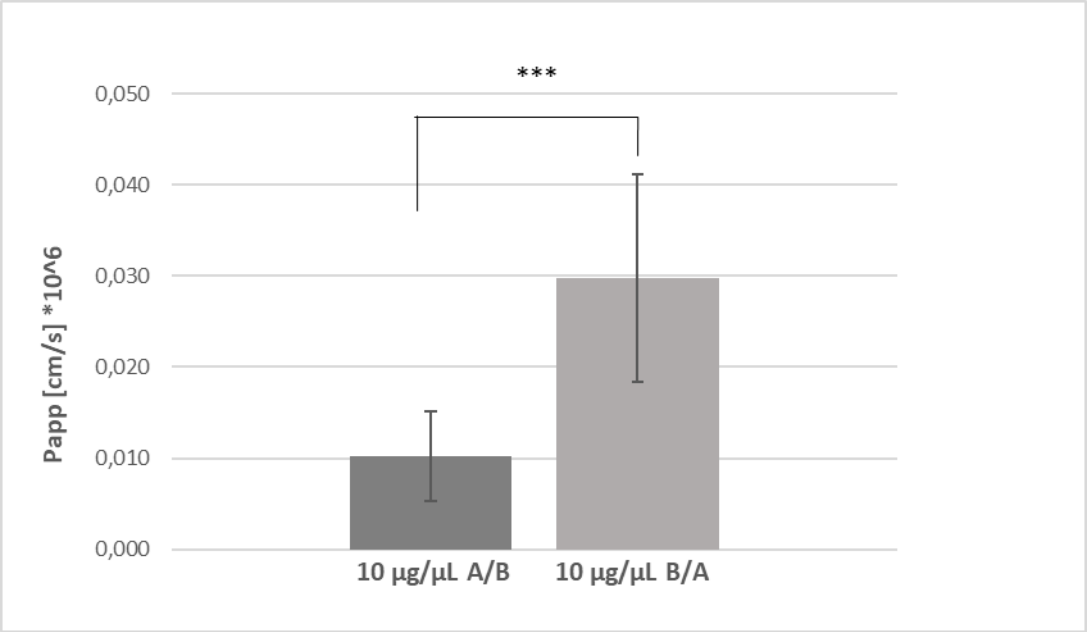

Figure 21. Apparent permeability coefficient P_{app} [cm/s] $*10^{-6}$ across the salivary gland epithelium model based on clone B2 of cell lineHTB-41, 10 µg/mL CRP in the apical-to basolateral direction (A/B) and in the basolateral-to apical direction (B/A) was applied. Data are shown as mean ± SD (n=3, N=4 per experiment). Statistical analysis was performed as Student´s t-test with α=0,05, $p < 0.05$ *, *p*<0.001***.

Table 28. The ratio of the B/A vs A/B direction for 10 µg/mL CRP in the salivary gland epithelium model HTB-41 based on clone B2. Data are displayed as mean ±SD (N=4) for all three independent experiments.

No. Transport study	CRP Concentration [µg/mL]	B/A vs A/B	
		mean	± SD
TS I	**10 µg/mL**	1,474	0,148
TS II	**10 µg/mL**	3,185	0,652
TS III	**10 µg/mL**	2,020	0,651
Summary TS I-III	**10 µg/mL**	**2,226**	**0,89**

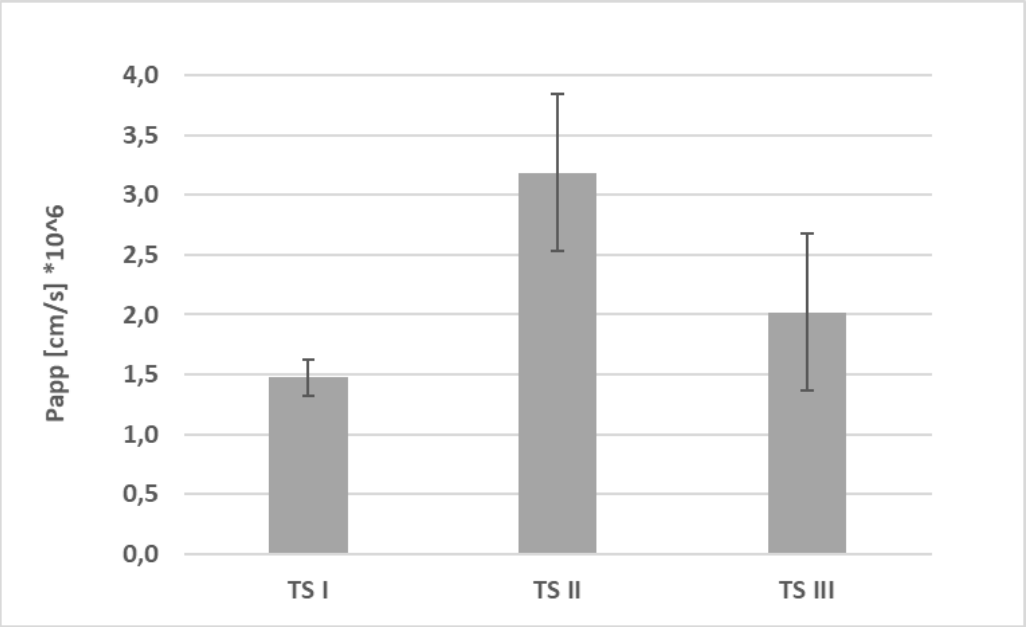

Figure 22. The ratio for 10 µg/mL CRP applied on the A/B and B/A directions in the salivary gland epithelium model based on clone B2 for all three independent experiments (N=4 per experiment). Values were showed as mean ± SD.

The B/A vs A/B ratio for C-reactive protein (CRP) were between 1,47 and 3,18 (Figure 22). Based on the graphic, comparing all three transport studies in the salivary gland epithelium model (clone B2), it could be suggest that there is an active transport for CRP across the *in vitro* model of the BSB. Summary of all data of the three transport studies revealed total B/A vs A/B ratio of 2,26 ± 0,89 for 10 µg/mL CRP clearly indicating a significant faster transport for CRP in the direction basolateral to apical (Table 28). Thus, it could be concluded thst an active transport system is present for CRP acros the submandibulary salivary gland model.

Table 29. Transepithelial electrical resistance (TEER) results showed as percent for the period 0 - 24 hours for C-reactive protein (CRP), concentration of 10 µg/mL in McCoy´s medium. The data is expressed as means ± SD of three independent experiments.

10 µg/mL CRP		**A/B**					**B/A**			
	Ωxcm² [0h]	**McCoy´s+; 0h [%]**		**McCoy´s+; 24h [%]**		**Ωxcm² [0h]**	**McCoy´s+; 0h [%]**		**McCoy´s+; 24h [%]**	
	mean	**mean**	**± SD**	**mean**	**± SD**	**mean**	**mean**	**± SD**	**mean**	**± SD**
TS I	**428 ±98,6**	**100%**	23,04%	**78,74%**	14,05%	**577,5 ± 55,4**	**100%**	9,60%	**66,15%**	4,09%
TS II	**440 ±77,3**	**100%**	17,56%	**61,87%**	12,46%	**561,9± 209,8**	**100%**	37,34%	**50,90%**	14,28%
TS II	**407,5 ±63,0**	**100%**	15,47%	**54,17%**	1,39%	**486,0 ± 124,4**	**100%**	25,59%	**51,01%**	16,66%

As showed in the table 29, TEER decreased between 54,17% to 78,74% for the apical-to basolateral direction (A/B), and values between 50,90 to 66,15% for the basolateral-to apical direction (B/A) for all three independent experiments after 24 hours incubation.

4.2.1. Regulation of RAGE after C-reactive protein transport studies

To examine a possible involvement and regulation of Receptor for Advanced Glycation endproducts (RAGE) by CRP, cell samples from the transport studies were analyzed and compared to untreated cell samples (controls) at the mRNA level.

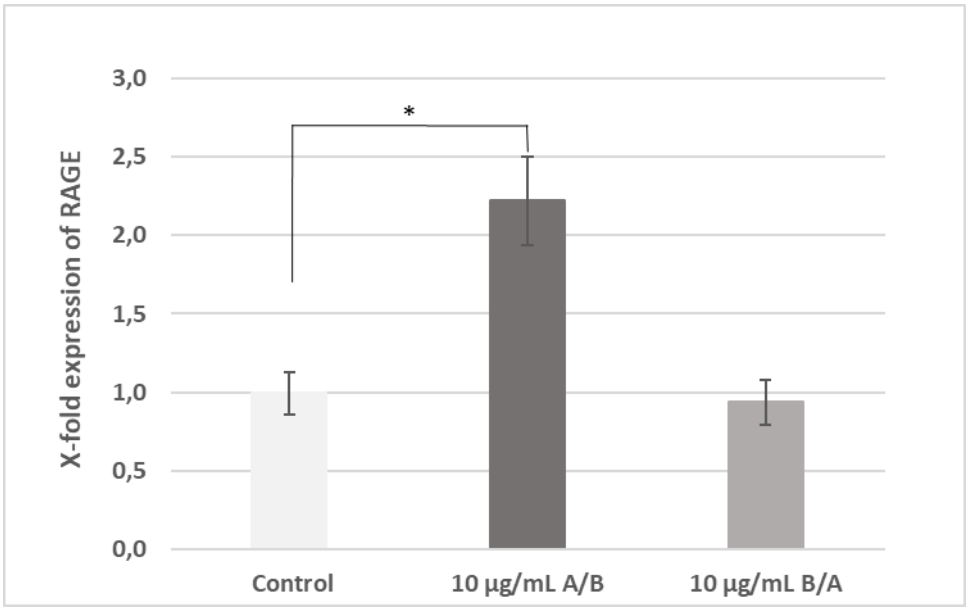

Figure 23. X-fold mRNA expression of RAGE from HTB-41 (B2 clone) treated with 10 µg/mL CRP. The values are shown as mean ± SD for three independent experiments (N=4 per experiment). Statistical analysis was performed using Student´s T-test, α=0.05, p<0,05*.

As shown in figure 23, 10 µg/mL CRP applied apically led to a significant 2,22 -fold upregulation of RAGE after 24 hours treatment.

4.3. Influence of soluble RAGE on CRP transport across HTB-41 (clone B2) cell layers

The optimized submandibular salivary gland barrier model based on clone B2 was used to investigate the influence of sRAGE on transport of CRP. CRP was applied either at apical or basolateral compartment at concentration of 10 µg/mL and was compared to CRP 10 µg/mL on the basolateral or apical side supplemented with 5 µg/mL sRAGE.

Table 30. Apparent permeability coefficient P_{app} [cm/s] $*10^{-6}$ values of 10 µg/mL CRP with 5 µg/mL soluble RAGE, obtained in the A/B direction and B/A direction. The data are expressed as mean± SD of two independent experiments (N=3-4 per experiment).

No. Transport study (TS)	Concentration [µg/mL]	Papp [cm/s] $*10^{-6}$ A/B	Papp [cm/s] $*10^{-6}$ B/A
		mean ± SD	mean ± SD
TS I	10 µg/mL CRP	0,040 ± 0,025	0,036 ± 0,015
	10 µg/mL CRP+5 µg/mLsRAGE	0,028 ± 0,005	0,078 ± 0,023
TS II	10 µg/mL CRP	0,019 ± 0,001	0,037 ± 0,012
	10 µg/mL CRP+5 µg/mLsRAGE	0,017± 0,005	0,072 ± 0,008
Summary TS I-II	**10 µg/mL CRP**	**0,031 ± 0,020**	**0,033 ± 0,013**
	10 µg/mL CRP+5 µg/mLsRAGE	**0,019 ± 0,011**	**0,075 ± 0,016**

The apparent permeability coefficient P_{app} for 10 µg/mL CRP after 24 hours showed an increased transport of CRP from A/B compared to the concentration of 10 µg/mL CRP supplemented with 5µg/mL sRAGE. Based on obtained results in the direction from basolateral to apical, there is a significant increase transport of CRP supplemented with 5µg/mL sRAGE.

In summary (Figure 24), comparing the transport studies I-II, all independent experiments showed an decreased transport of 10 µg/mL CRP with 5µg/mL sRAGE in the direction apical to basolateral (A/B) and a significant increased transport of 10 µg/mL CRP with 5 µg/mL soluble RAGE from basolateral-to apical direction (B/A) (p<0,01) compared to the transport of 10 µg/mL CRP without sRAGE. Also, it was shown that the novel salivary gland epithelium model based on clone B2 was applicable to study the transport of the salivary biomarker CRP with and without soluble receptor for advance glycation end products (sRAGE).

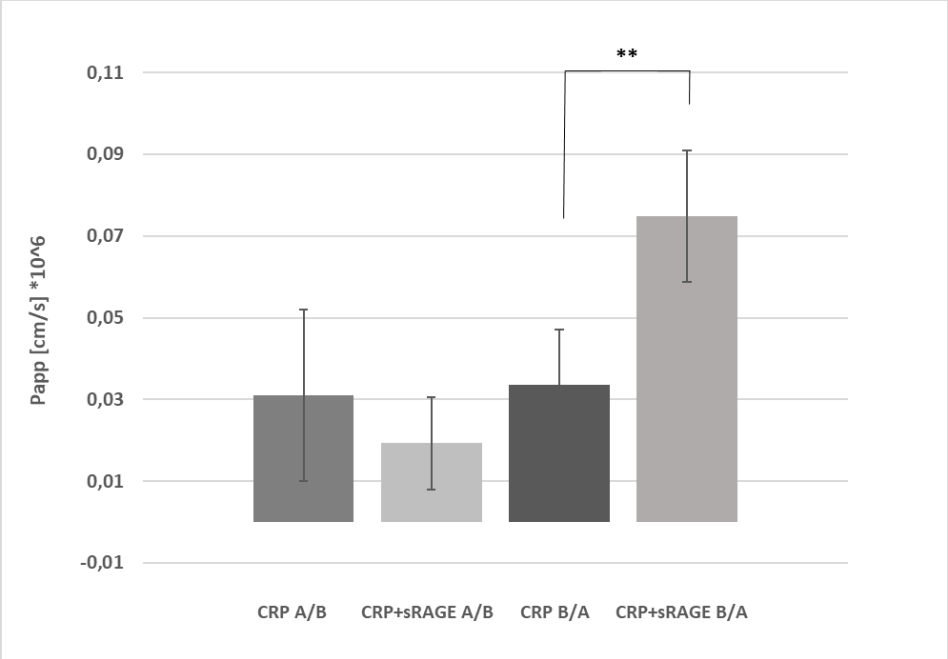

Figure 24. Apparent permeability coefficient P_{app} [cm/s] $*10^{-6}$ across the salivary gland epithelium model based on clone B2, in the presence of 10 µg/mL CRP and 10 µg/mL CRP supplemented with 5% sRAGE, in the apical to basolateral (A/B) and basolateral to apical direction (B/A). Data are showed as mean ± SD. The statistical significance p< 0,01 **, was calculated using the student´s t -test, α=0.05.

Table 31. Transepithelial electrical resistance (TEER) results showed as percent for the time interval 0- 24 hours for 10 µg/mL CRP and for 10 µg/mL CRP supplemented with 5µg/mL soluble RAGE in HTB-41 (clone B2) cell line.

		A/B					B/A			
	Ωxcm²	**McCoy´s+; 0h**		**McCoy´s+; 24h**		**Ωxcm²**	**McCoy´s+; 0h**		**McCoy´s+; 24h**	
10 µg/mL CRP	**mean±SD**	**mean**	**± SD**	**mean**	**± SD**	**mean±SD**	**mean**	**± SD**	**mean**	**± SD**
TS I	**428,9±53,2**	**100%**	12,39%	**43,99%**	7,56%	**705,2±171,2**	**100%**	24,28%	**47,22%**	8,85%
TS II	**444,7±48,6**	**100%**	10,93%	**27,26%**	4,43%	**644,2±85,3**	**100%**	13,23%	**14,75%**	2,88%
10 µg/mL CRP + 5µg/mL sRAGE										
TS I	**735,4±134,7**	**100%**	18,32%	**40,22%**	5,76%	**503,2±149,8**	**100%**	29,76%	**40,50%**	7,69%
TS II	**638,7±101,0**	**100%**	15,81%	**20,08%**	2,79%	**437,6±42,6**	**100%**	9,73%	**19,04%**	3,19%

As showed in the table 31, the TEER values at time zero were set as 100 % (percentage of highest), before adding 10 µg/mL CRP, or 10 µg/mL CRP supplemented with 5µg/mL soluble RAGE. After 24 hours measuring the TEER showed a similar decrease of the values for CRP and CRP supplemented with sRAGE at both directions apical to basolateral (A/B) and basolateral to apical (B/A).

4.4. Influence of soluble RAGE on CRP transport across TR146 cell layers

To investigate the influence of RAGE on the transport of CRP, transport studies were performed with 10 µg/mL CRP supplemented with 5 µg/mL soluble RAGE applied on the apical or basolateral side in the oral mucosa model (TR146 cell line) and compared to the permeability of 10 µg/mL CRP alone for each experiment.

Table 32. Apparent permeability coefficient P_{app} [cm/s] $*10^6$ values, for 10 µg/mL CRP and 10 µg/mL CRP supplemented with 5µg/mL sRAGE, obtained in the A/B direction and B/A direction. The data are expressed as means ± SD of two independent experiments (n=3-4 per experiment).

No. Transport study (TS)	Concentration [µg/mL]	Papp [cm/s] $*10^{-6}$ A/B	Papp [cm/s] $*10^{-6}$ B/A	Student´s t-test
		mean ± SD	mean ± SD	mean
TS I	**10 µg/mL CRP**	0,20 ± 0,01	0,25 ± 0,04	0,04
	10 µg/mL CRP+5 µg/mL sRAGE	0,13 ± 0,07	0,21 ± 0,11	0,02
TS II	**10 µg/mL CRP**	0,07 ± 0,01	0,14 ± 0,01	0,001
	10 µg/mL CRP+5 µg/mL sRAGE	0,10 ± 0,03	0,14 ± 0,01	0,18
Summary TS I-II	**10 µg/mL CRP**	**0,015 ± 0,07**	**0,19 ± 0,07**	**0,189**
	10 µg/mL CRP+5 µg/mL sRAGE	**0,12 ± 0,03**	**0,17 ± 0,05**	**0,038**

Regarding the independent experiments, the calculated apparent permeability coefficient P_{app} after 24 hours, showed an increased transport of CRP from basolateral to apical side (B/A), at 10 µg/mL CRP concentration, compared to the direction from apical to basolateral side (A/B).

Addition of soluble RAGE decrease the permeability of CRP form 0,15 ± 0,07 cm/s $*10^{-6}$ to 0,12 ± 0,03 cm/s $*10^{-6}$ for transport studies from apical to basolateral (A/B) and from 0,19 ± 0,07 cm/s $*10^{-6}$ to 0,17 ± 0,05 cm/s $*10^{-6}$ for transport studies from basolateral to apical (B/A) (Table 32, Figure 25).

As showed in table 33, the TEER values at time zero were seta as 100 %, before adding 10 µg/mL CRP, or 10 µg/mL CRP supplemented with 5 µg/mL sRAGE. After 24 hours TEER values was decreased between 16,25% to 32,95% by adding only CRP, and for CRP supplemented with sRAGE TEER values were between 17,61% and 30,71%.

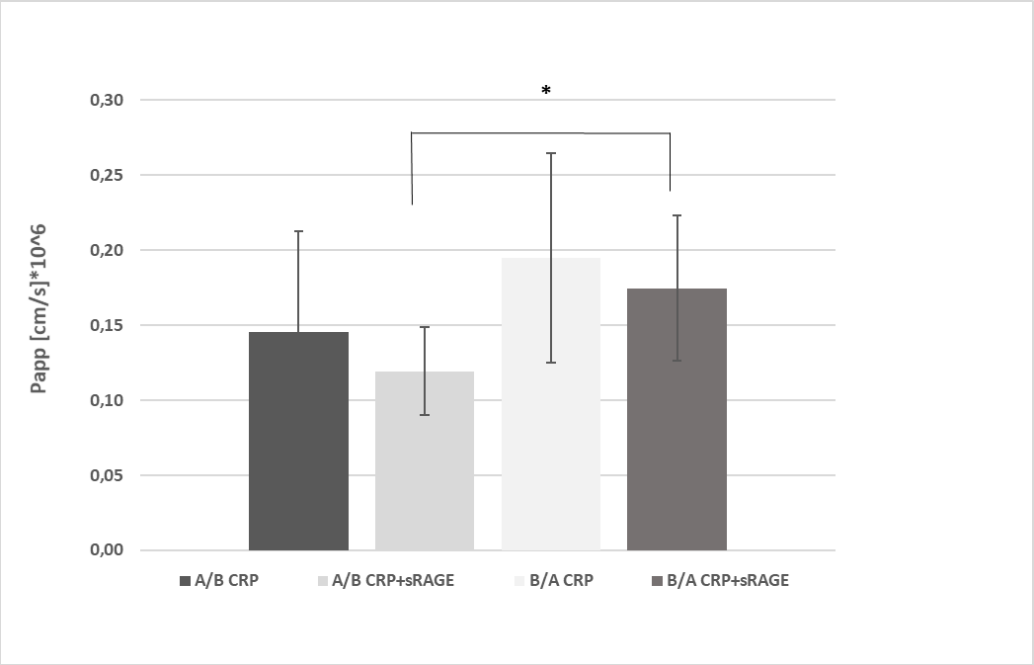

Figure 25. Apparent permeability P_{app}[cm/s] $*10^{-6}$ values of the oral mucosa upon applying 10 µg/mL CRP and 10 µg/mL CRP supplemented with 5 µg/mL soluble RAGE on the apical (A/B) or basolateral (B/A) side for 24 hours. Results shown as mean ± SD of two independent experiments (N=3-4 per experiment). Statistical analysis was performed as student´s t-test, α=0.05, *p*<0.05*.

Table 33: Transepithelial electrical resistance (TEER) results showed as percent for the time interval 0- 24 hours for 10 µg/mL CRP and for 10 µg/mL CRP supplemented with 5µg/mL soluble RAGE in HBSS medium

		A/B				B/A				
	Ωxcm2	**HBSS; 0h**		**HBSS; 24h**		**Ωxcm2**	**HBSS; 0h**		**HBSS; 24h**	
10 µg/mL CRP	**mean±SD**	**mean**	**± SD**	**mean**	**± SD**	**mean±SD**	**mean**	**± SD**	**mean**	**± SD**
TS I	**300,9±94,1**	**100%**	31,29%	**16,25%**	1,88%	**202,2±42,9**	**100%**	21,22%	**30,62%**	7,29%
TS II	**174,6±15,5**	**100%**	8,88%	**32,87%**	2,54%	**197,1±24,5**	**100%**	12,44%	**32,95%**	3,51%
10 µg/mL CRP + 5µg/mL sRAGE										
TS I	**222,4±23,5**	**100%**	10,56%	**28,58%**	3,43%	**267,8±24,2**	**100%**	9,04%	**17,61%**	3,41%
TS II	**221,6±37,8**	**100%**	17,06%	**30,71%**	8,70%	**240,5±28,2**	**100%**	11,73%	**27,43%**	1,77%

5. Discussion

Despite the regular screening and check-ups, many diseases are undetected until a late phase where morbid symptoms become apparent. To overcome these challenges, researchers are working on biomarkers to detect the diseases in early stages.

Over the past years, saliva has gained attention as a diagnostic fluid, because saliva offers advantage over serum. (Pfaffe *et al*., 2011). Saliva as a diagnostic tool should be used due to a multitude of compelling advantages, safer to administrate than serum sampling, minimal risk of cross-contamination, and all these advantages make saliva an appealing diagnostic candidate for the detection and monitoring of several biomarkers in infants, children, adults and uncooperative patients and in many circumstances in which blood sampling is not available (Chiappin *et al*., 2007). Like serum, saliva contains hormones, antibodies, growth factors, enzymes, microbes, and their products. For example, biomolecules enter the saliva compartment from blood by passive diffusion (lipophilic molecules such as steroid hormones), active transport of proteins via ligand-receptor binding or extracellular ultrafiltration (filtration through the spaces between acinus and ductal cells) and endocytosis. Therefore, in many cases, saliva reflects the physiological function of the body (Pfaffe *et al*., 2011).

In biomarker research, transport studies across salivary gland models could be used to verify the validity of a salivary biomarker. Understanding the transport of a salivary biomarker across the BSB could provide the causal link between the saliva and the blood concentration of the respective biomarker.

The transport of ferritin, associated with iron storage in serum (Walters *et al.,*1973), and C-reactive protein (CRP) associated with acute inflammatory response in serum (Ouellet-Morin, Danese, Williams & Arseneault, 2011) were investigated in this thesis. For this, cell models of the oral mucosa based on the human buccal mucosa carcinoma cell line TR146 and HTB-41 (clone B2) as submandibular salivary gland model were selected (Lin *et al*., 2020a; Lin *et al.,* 2020b). TR146 are sed as an *in vitro* culture model to study buccal drug delivery, including ionized drugs, and also for permeability studies (Jacobsen *et al*., 1999; Nielsen *et al*., 1999; Nielsen *et al*., 2000).

Serum ferritin is also a well-known inflammatory marker (Kell &Pretorius, 2014) and elevated serum levels of ferritin were measured in patients with anemia, diabetes or periodontitis, correlating with salivary ferritin levels (Jagannathan *et al*., 2012; Mishra *et al*., 1992).

As ferritin was also detected in saliva and saliva´s accessibility is easy and non-invasive, this fluid has gained more interest in using for example salivary ferritin as a biomarker. A correlation between serum ferritin and salivary ferritin has been already observed, particularly in iron overload disorder (Jagannathan*, et al*., 2012).

As clinical concentrations of ferritin of 30-300 ng/mL are considered normal for male and 10-200 ng/ml for women. Almost half of patients with chronic kidney disease on maintenance hemodialysis have a serum ferritin > 500 ng/mL. Increased ferritin levels in hemodialysis patients are probably the results of inflammation. Hemodialysis patients with serum ferritin > 800 ng/mL had a higher CRP level. Serum ferritin levels greater than 1000 ng/mL are a nonspecific marker of illness, infection and cancer (Wang *et al*., 2010).

Based on this 300 ng/mL and 1000 ng/mL ferritin was chosen for our studies and were applied either on the apical or basolateral side. After 24 hours incubation sufficient amounts of ferritin were detected on each opposite side, although no significant concentration or permeation direction dependent effects were found in the salivary gland model. In our models, the tendency to permeate faster into the saliva compartment was detected for ferritin. According to this, in the oral mucosa model (TR146 cell line), ferritin (300 ng/mL and 1000 ng/mL applied) permeated significantly faster from the blood (basolateral compartment) to the saliva (apical side), comparing to the other direction (A/B) (Figure 15). In the submaxillary gland model (B2 clone), for both concentrations (300 ng/mL and 1000 ng/mL applied) after 24 hours the calculated apparent permeability P_{app} showed a higher, but not statistically significant permeation of ferritin from the blood (apical side) to the saliva (basolateral compartment), comparing to the other direction (B/A) (Figure 18).

Studies across both BSB models indicated the general tendency for ferritin to be transported faster from blood to saliva and suggested the suitability of ferritin as salivary biomarker. Different transport data in both models indicate the need to try even lower concentration. Levels lower than 30 ng/mL were postulated to be an indicator for iron deficiency.

Recent studies have also shown that transferrin receptor (TfR) play an important role in the endocytosis at the oral epithelium, and that the uptake of eg. Periodontal pathogen (*Porphyromonas gingivalis*) and nanoparticles (decorated with transferrin) were mediated by the transferrin receptor (TfR). It was also shown that ferritin was uptaken from light and dark cells of the submandibular gland after injection, ferritin to the main excretory duct of the rat submandibular gland (Bierbaumer *et al*., 2018), suggesting a correlation between ferritin uptake and TfR activity.

It was hypothesized that the postulated transport mechanism of ferritin via TfR-1 across blood-brain barrier (BBB) might also work at the BSB. To investigate these transport mechanisms, it was aimed to analyze the expression of the transferrin receptor (TfR) in TR146 cell (the oral mucosa model) and HTB-41 (clone B2) cells after treatment with ferritin.

Interestingly, the addition of ferritin changed transferrin receptor (TfR) expression of both cell lines in a different manner. Expression of TfR of ferritin treated HTB-41 (clone B2) cells was significantly decreased in both directions and applied concentrations in comparison to untreated control (Figure 20).

Treatment of the TR146 cells with ferritin, shows in contrast to HTB-41 (clone B2) an upregulation at the mRNA level of TfR compared to the untreated control (Figure 17). The difference between treated and untreated is not increased at HTB-41 (clone B2) cells. However, a correlation between the treatment directions could not be shown. Why the different transport models show opposite regulation of TfR is still unclear and will need more investigations. Different transport data in both models indicate the need and importance to involve models of several parts of the blood-saliva barrier (BSB) for comprehensive biomarker studies, and further studies are needed to elucidate the mechanisms and regulation of ferritin transport in detail.

CRP is a commonly used marker of inflammation, measured in serum blood sample. Serum C-reactive protein (CRP) detected in 1930´s, its values as an early marker of bacterial infection has been documented in screening for bacteremia in children, infection in leukemic patients, in neonatal septicemia, postsurgical infections (Lindbäck *et al.,* 1989). CRP as an inflammatory marker found in blood plasma and shows a high level of up to > 10 mg/mL in patients with cardiovascular disease (Dhingra *et al.,* 2007). Recently, an increased level of CRP has shown an

association with faster progression of Amyotrophic Lateral Sclerosis (ALS) compared to patients with lower CRP levels (Lunetta *et al.,* 2017).

To study the transport mechanism of CRP using *in vitro* models of the BSB, 10 µg/mL CRP was used, as clinical concentrations of 10-20 µg/mL have been proven in previous studies to affect in vitro models of the BBB (Kuhlmann *et al*., 2009). Applying CRP in our salivary gland model (clone B2), either on the apical side or basolateral side, all three individual transport studies showed a faster transport from the basolateral to the apical (B/A) side (Figure 21). This indicates a preferred transport direction from blood to saliva supporting CRP as a salivary biomarker. Since there is literature data linking RAGE and CRP (Yan, Bierhaus, Nawroth and Stern, 2009), the expression of RAGE at the mRNA level after CRP treatment was also tested. The results showed a downregulation of the mRNA expression of RAGE on the basolateral side and an upregulation on the apical side (Figure 23).

A possible involvement of RAGE in separate transport studies with CRP was also analyzed. For this, soluble RAGE (sRAGE) was applied to CRP transport studies in our mucosal and salivary gland model. The addition of soluble RAGE in the salivary gland model resulted in a reduced transport rate from apical to basolateral (blood to saliva), but to an increased transport rate from basolateral to apical (saliva to blood) (Figure 24). The addition of sRAGE showed a RAGE-dependent CRP transport mechanism for the salivary gland model by influencing the transport of CRP to saliva and limiting the transport to the blood side. In the oral mucosa model, addition of soluble RAGE decreased the permeability of CRP transported from the apical to basolateral (A/B) side as well as from the basolateral to apical (B/A) side (Figure 25).

Based on the results obtained from the transport studies with 10 µg/mL CRP or 10 µg/mL CRP with 5µg/mL soluble RAGE in saliva, both models of the BSB, representing the oral mucosa and submandibular salivary gland, showed an elevated transport of CRP in the direction from blood to saliva.

While an elevated transport from blood to saliva was shown in this study, and the influence of RAGE on CRP transport, further studies would improve our current knowledge and strengthen the relevance of CRP as salivary biomarker.

6. Conclusion

The study of ferritin transport across the *in vitro* models of the salivary gland, showed that the novel salivary gland epithelium model based on clone B2 was applicable to study the transport of the salivary biomarkers. A correlation between the treatment directions (with ferritin) could not be shown.

The study of transport mechanism of CRP using established *in vitro* models of the blood-saliva barrier (BSB) showed a faster CRP transport in the direction from blood to saliva, supporting its feasibility as a salivary marker. Based on the *in vitro* data from the transport studies, also with soluble RAGE, both *in vitro* models showed an involvement of RAGE in the transport of CRP.

7. References

Ahsan H. Biomolecules and biomarkers in oral cavity: bioassays and immunopathology. *J* Immunoassay Immunochem. 2019;40(1):52-69. doi:10.1080/15321819.2018.1550423

Agarwal P.K., Agarwal K.N., Agarwal D.K. Biochemical changes in saliva of malnourished children. Am J Clin Nutr. 1984;39(2):181-184. doi:10.1093/ajcn/39.2.181

Apodaca G. Endocytic traffic in polarized epithelial cells: role of the actin and microtubule cytoskeleton. Traffic. 2001;2(3):149-59. doi: 10.1034/j.1600-0854.2001.020301.x. PMID: 11260520.

Arnold R.R., Ribeiro A.A. Introduction to the Oral Cavity. In: Azcarate-Peril M., Arnold R., Bruno-Bárcena J. (eds) How Fermented Foods Feed a Healthy Gut Microbiota. Springer, Cham.2019. Available from: https://doi.org/10.1007/978-3-030-28737-5_6

Baker O.J. Tight junctions in salivary epithelium. J Biomed Biotechnol. 2010; 2010:278948; PMID:20182541; http://dx.doi.org/10.1155/2010/278948

Bruewer M., Nusrat A. Regulation of Paracellular Transport across Tight Junctions by the Actin Cytoskeleton. In: Madame Curie Bioscience Database [Internet]. Austin (TX): Landes Bioscience; 2000-2013. Available from: https://www.ncbi.nlm.nih.gov/books/NBK6487/

Bierhaus A., Humpert P.M., Morcos M., et al. Understanding RAGE, the receptor for advanced glycation end products. J Mol Med 83, 2005; 876–886; https://doi.org/10.1007/s00109-005-0688-7

Bierbaumer L., Schwarze U.Y., Gruber R., Neuhaus W. Cell culture models of oral mucosal barriers: A review with a focus on applications, culture conditions and barrier properties. Tissue Barriers. 2018;6(3):1479568. doi:10.1080/21688370.2018.1479568

Bhusnure O.G, et al. Ijppr.Human, 2017; Vol. 10 (1): 118-131

Califf R. M. Biomarker definitions and their applications. Exp Biol Med (Maywood). 2018;243(3):213-221. doi:10.1177/1535370217750088

Chen J., Huang L., Song M., Yu S., Gao P., & Jing J. C-reactive protein upregulates receptor for advanced glycation end products expression and alters antioxidant defenses in rat endothelial progenitor cells. Journal of cardiovascular pharmacology, 2009, 53(5), 359–367; https://doi.org/10.1097/FJC.0b013e31819b5438

Chen J., Jin J., Song M., Dong H., Zhao G. & Huang L. C-reactive protein down-regulates endothelial nitric oxide synthase expression and promotes apoptosis in endothelial progenitor cells through receptor for advanced glycation end-products. Gene, 2012; 496(2), 128–135. https://doi.org/10.1016/j.gene.2011.12.039

Chiappin S., Antonelli G., Gatti R., De Palo E.F. Saliva specimen: a new laboratory tool for diagnostic and basic investigation. Clin Chim Acta.2007; 383(1-2):30-40. doi:10.1016/j.cca.2007.04.011

Dillon M. C., Opris D. C., Kopanczyk R., Lickliter J., Cornwell H. N., Bridges E. G., Nazar A. M., & Bridges K. G. Detection of homocysteine and C-reactive protein in the saliva of healthy adults: comparison with blood levels. Biomarker insights, 2010; 5, 57–61. https://doi.org/10.4137/bmi.s5305

Du W., Fan Y., Zheng N., et al. Transferrin receptor specific nanocarriers conjugated with functional 7peptide for oral drug delivery. Biomaterials. 2013;34(3):794-806. doi:10.1016/j.biomaterials.2012.10.003

Dhingra R., Gona P., Nam B.H., et al. C-reactive protein, inflammatory conditions, and cardiovascular disease risk.Am J Med. 2007;120(12):1054-1062. doi:10.1016/j.amjmed.2007.08.037

FDA-NIH Biomarker Working Group. BEST (Biomarkers, EndpointS, and other Tools) Resource [Internet]. Silver Spring (MD): Food and Drug Administration (US); 2016-. Monitoring Biomarker. 2016; Available from: https://www.ncbi.nlm.nih.gov/books/NBK402282/ Co-published by National Institutes of Health (US), Bethesda (MD).

International Transport Consortium, Giacomini K.M., Huang S.M., et al. Membrane transporters in drug development. Nat Rev Drug Discov. 2010;9(3):215–236. https://doi.org/10.1038/nrd3028

Garrod D, Chidgey M. Desmosome structure, composition and function. Biochim Biophys Acta. 2008;1778(3):572-587. doi:10.1016/j.bbamem.2007.07.014

Groeger S., Meyle J. Oral Mucosal Epithelial Cells. Front Immunol. 2019; 10:208. doi:10.3389/fimmu.2019.00208

Giard D.J., Aaronson S.A., Todaro G.J., et al. In vitro cultivation of human tumors: establishment of cell lines derived from a series of solid tumors. J Natl Cancer Inst. 1973; 51(5):1417-1423. doi:10.1093/jnci/51.5.1417

Hartsock A., Nelson W.J. Adherens and tight junctions: structure, function and connections to the actin cytoskeleton. Biochim Biophys Acta. 2008;1778(3):660-669. doi:10.1016/j.bbamem.2007.07.012

Hovav A.H. Dendritic cells of the oral mucosa. Mucosal Immunol. 2014;7(1):27–37. doi:10.1038/mi.2013.42

Holmberg K. V., & Hoffman M. P. Anatomy, biogenesis and regeneration of salivary glands. Monographs in oral science. 2014; 24, 1–13. https://doi.org/10.1159/000358776

Humphrey S.P., Williamson R.T. A review of saliva: normal composition, flow, and function. J Prosthet Dent. 2001;85(2):162-169. doi:10.1067/mpr.2001.113778

Ivanov A.I., Nusrat A., Parkos C.A. Endocytosis of the apical junctional complex: mechanisms and possible roles in regulation of epithelial barriers. Bioessays. 2005;27(4):356-65. doi: 10.1002/bies.20203.PMID: 15770686.

Iorgulescu G. Saliva between normal and pathological. Important factors in determining systemic and oral health. J Med Life. 2009;2(3):303-307.

Jagannathan N., Thiruvengadam C., Ramani P., Premkumar P., Natesan A., Sherlin H.J. Salivary ferritin as a predictive marker of iron deficiency anemia in children. J Clin Pediatr Dent. 2012;37(1):25-30. doi:10.17796/jcpd.37.1.ap2054376201537

Jacobsen J., Nielsen E.B., Brøndum-Nielsen K., et al. Filter-grown TR146 cells as an in vitro model of human buccal epithelial permeability. Eur J Oral Sci. 1999;107(2):138-146. doi:10.1046/j.0909-8836.1999.eos107210.x

Kell D.B, Pretorius E. Serum ferritin is an important inflammatory disease marker, as it is mainly a leakage product from damaged cells. Metallomics. 2014;6(4):748-73. doi: 10.1039/c3mt00347g. PMID: 24549403.

Brij Kumar, Nilotpol Kashyap, Alok Avinash, Ramakrishna Chevvuri, Mylavarapu Krishna Sagar, Kumar Shrikant, “The composition, function and role of saliva in maintaining oral health: A review,” Int J Contemp Dent Med Rev.2017, Article ID: 011217, 2017. doi: 10.15713/ins.ijcdmr.121

Khan AI, Liu J, Dutta P. Iron transport kinetics through blood-brain barrier endothelial cells. Biochim Biophys Acta Gen Subj. 2018;1862(5):1168-1179. doi:10.1016/j.bbagen.2018.02.010

Kuhlmann C.R., Librizzi L., Closhen D., et al. Mechanisms of C-reactive protein-induced blood-brain barrier disruption. Stroke. 2009;40(4):1458-66. doi: 10.1161/STROKEAHA.108.535930.

Laffleur F. Mucoadhesive polymers for buccal drug delivery. Drug Development and Industrial Pharmacy,2014;40:5,591-598;DOI:10.3109/03639045.2014.892959; https://doi.org/10.3109/03639045.2014.892959

Li L, Fang CJ, Ryan JC, et al. Binding and uptake of H-ferritin are mediated by human transferrin receptor-1. Proc Natl Acad Sci U S A. 2010;107(8):3505-3510. doi:10.1073/pnas.0913192107

Li Y., Lu J., & Paxton J. W. The role of ABC and SLC transporters in the pharmacokinetics of dietary and herbal phytochemicals and their interactions with xenobiotics. Current drug metabolism. 2012; 13(5), 624–639. https://doi.org/10.2174/1389200211209050624

Lin G.C., Leitgeb T., Vladetic A., et al. Optimization of an oral mucosa in vitro model based on cell line TR146 [published correction appears in Tissue Barriers. 2020 Jul 2;:1784644]. Tissue Barriers. 2020;8(2):1748459. doi:10.1080/21688370.2020.1748459; (a)

Lin G.C., Smajlhodzic M., Bandian A.M., et al. An In Vitro Barrier Model of the Human Submandibular Salivary Gland Epithelium Based on a Single Cell Clone of Cell Line HTB-41: Establishment and Application for Biomarker Transport Studies. Biomedicines. 2020;8(9):302. Published 2020 Aug 23. doi:10.3390/biomedicines8090302 (b)

Lin L., Yee S.W., Kim R.B., Giacomini K.M. SLC transporters as therapeutic targets: emerging opportunities. Nat Rev Drug Discov. 2015;14(8):543-560. doi:10.1038/nrd4626

Lindbäck S., Hellgren U., Julander I., Hansson L.O. The value of C-reactive protein as a marker of bacterial infection in patients with septicaemia/endocarditis and influenza. Scand J Infect Dis. 1989;21(5):543-9. doi: 10.3109/00365548909037883. PMID: 2587955.

Lodish H., Berk A., Zipursky S.L., et al. Molecular Cell Biology. 4th edition. New York: W. H. Freeman; 2000. Section 15.7, Transport across Epithelia. Available from: https://www.ncbi.nlm.nih.gov/books/NBK21502/

Lunetta C., Lizio A., Maestri E., et al. Serum C-Reactive Protein as a Prognostic Biomarker in Amyotrophic Lateral Sclerosis. JAMA Neurol. 2017;74(6):660-667. doi:10.1001/jamaneurol.2016.6179

Mahajan N., Bahl A., Dhawan V. C-reactive protein (CRP) up-regulates expression of receptor for advanced glycation end products (RAGE) and its inflammatory ligand EN-RAGE in THP-1 cells: inhibitory effects of atorvastatin. Int J Cardiol. 2010;142(3):273-278. doi:10.1016/j.ijcard.2009.01.008

Mitul P., et al. Buccal drug delivery system: the current interest. International Research Journal of Pharmacy. 2011;2(12):4-11

Mishra O.P., Agarwal K.N., Agarwal R.M. Salivary iron status in children with iron deficiency and iron overload. J Trop Pediatr. 1992;38(2):64-7. doi: 10.1093/tropej/38.2.64. PMID: 1569637.

Mørck Nielsen H., Rømer Rassing M. TR146 cells grown on filters as a model of human buccal epithelium: V. Enzyme activity of the TR146 cell culture model, human buccal epithelium and porcine buccal epithelium, and permeability of leu-enkephalin. Int J Pharm. 2000;200(2):261-270. doi:10.1016/s0378-5173(00)00394-x

Nielsen H.M., Rassing M.R. TR146 cells grown on filters as a model of human buccal epithelium: III. Permeability enhancement by different pH values, different osmolality values, and bile salts. Int J Pharm. 1999;185(2):215-225. doi:10.1016/s0378-5173(99)00165-9

Ouellet-Morin I., Danese A., Williams B., Arseneault L. Validation of a high-sensitivity assay for C-reactive protein in human saliva. Brain Behav Immun. 2011;25(4):640-6. doi: 10.1016/j.bbi.2010.12.020. PMID: 21236331.

Patel V.F., Liu F., Brown M.B. Advances in oral transmucosal drug delivery. J Control Release. 2011;153(2):106-116. doi:10.1016/j.jconrel.2011.01.027

Pay J.B., Shaw A.M. Towards salivary C-reactive protein as a viable biomarker of systemic inflammation. Clin Biochem. 2019; 68:1-8. doi:10.1016/j.clinbiochem.2019.04.006

de Paula F., Teshima T.H.N., Hsieh R., Souza M.M., Nico M.M.S., Lourenco S.V. Overview of Human Salivary Glands: Highlights of Morphology and Developing Processes. Anat Rec (Hoboken). 2017;300(7):1180–1188. doi:10.1002/ar.23569

Pfaffe T., Cooper-White J., Beyerlein P., Kostner K., Punyadeera C. Diagnostic Potential of Saliva: Current State and Future Applications. Clinical Chemistry. 2011;57(5):675–687, https://doi.org/10.1373/clinchem.2010.153767

Punj A. Secretions of Human Salivary Gland. In Salivary Glands - New Approaches in Diagnostics and Treatment. IntechOpen, London; 2019; 3-13. https://doi.org/10.5772/intechopen.75538

Seeger M. A., & van Veen H. W.Molecular basis of multidrug transport by ABC transporters. Biochimica et biophysica acta, 2009; 1794(5):725–737. https://doi.org/10.1016/j.bbapap.2008.12.004

Squier C.A., Kremer M.J. Biology of oral mucosa and esophagus. J Natl Cancer Inst Monogr. 2001;(29):7–15. doi: 10.1093/oxfordjournals.jncimonographs.a003443

Tsukita S., Furuse M., Itoh M. Multifunctional strands in tight junctions. Nat Rev Mol Cell Biol. 2001;2(4):285-293. doi:10.1038/35067088

van Meer G., Simons K. The function of tight junctions in maintaining differences in lipid composition between the apical and the basolateral cell surface domains of MDCK cells. EMBO J. 1986;5(7):1455–1464.

Walters G.O., Miller F.M., Worwood M. Serum ferritin concentration and iron stores in normal subjects. J Clin Pathol. 1973;26(10):770-2. doi: 10.1136/jcp.26.10.770. PMID: 4750458; PMCID: PMC477879.

Wang W., Knovich M.A., Coffman L.G., Torti F.M., Torti S.V. Serum ferritin: Past, present and future. Biochim Biophys Acta. 2010;1800(8):760-769. doi:10.1016/j.bbagen.2010.03.011

WHO International Programme on Chemical Safety. Biomarkers and Risk Assessment: Concepts and Principles. http://www.inchem.org/documents/ehc/ehc/ehc155.htm (accessed 1993)

Yan S.D., Bierhaus A., Nawroth P.P., Stern D.M. Endothelial precursor cells and CRP on the RAGE: activation or cell death? J Cardiovasc Pharmacol. 2009;53(5):349-51. doi: 10.1097/FJC.0b013e31819d6188. PMID: 19276986.

Yoshizawa J.M., Schafer C.A., Schafer J.J., Farrell J.J., Paster B.J., Wong D.T. Salivary biomarkers: toward future clinical and diagnostic utilities. Clin Microbiol Rev. 2013;26(4):781-91. doi: 10.1128/CMR.00021-13. PMID: 24092855; PMCID: PMC3811231.

Zihni C., Mills C., Matter K., Balda M.S. Tight junctions: from simple barriers to multifunctional molecular gates. Nat Rev Mol Cell Biol. 2016;17(9):564-580. doi:10.1038/nrm.2016.80

Zhong Y., Li S.H., Liu S.M., et al. C-Reactive protein upregulates receptor for advanced glycation end products expression in human endothelial cells. Hypertension. 2006;48(3):504-511. DOI: 10.1161/01.hyp.0000234904.43861.f7